energies

MDPI

Article

# Application of a Simplified Thermal-Electric Model of a Sodium-Nickel Chloride Battery Energy Storage System to a Real Case Residential Prosumer

**Fabio Bignucolo [1,*], Massimiliano Coppo [1], Giorgio Crugnola [2] and Andrea Savio [1]**

1 Department of Industrial Engineering, University of Padova, 35131 Padova, Italy; massimiliano.coppo@unipd.it (M.C.); andrea.savio.1@unipd.it (A.S.)
2 FZSONICK SA, Via Laveggio 15, 6855 Stabio, Switzerland; giorgio.crugnola@fzsonick.com
* Correspondence: fabio.bignucolo@unipd.it; Tel.: +39-049-827-7585

Received: 1 August 2017; Accepted: 21 September 2017; Published: 26 September 2017

**Abstract:** Recently, power system customers have changed the way they interact with public networks, playing a more and more active role. End-users first installed local small-size generating units, and now they are being equipped with storage devices to increase the self-consumption rate. By suitably managing local resources, the provision of ancillary services and aggregations among several end-users are expected evolutions in the near future. In the upcoming market of household-sized storage devices, sodium-nickel chloride technology seems to be an interesting alternative to lead-acid and lithium-ion batteries. To accurately investigate the operation of the $NaNiCl_2$ battery system at the residential level, a suitable thermoelectric model has been developed by the authors, starting from the results of laboratory tests. The behavior of the battery internal temperature has been characterized. Then, the designed model has been used to evaluate the economic profitability in installing a storage system in the case that end-users are already equipped with a photovoltaic unit. To obtain realistic results, real field measurements of customer consumption and solar radiation have been considered. A concrete interest in adopting the sodium-nickel chloride technology at the residential level is confirmed, taking into account the achievable benefits in terms of economic income, back-up supply, and increased indifference to the evolution of the electricity market.

**Keywords:** $NaNiCl_2$ batteries; photovoltaic generation; residential end-users; self-consumption; sodium-nickel chloride technology; techno-economic analysis

## 1. Introduction

The climate changes experienced in the last decades and the ever-increasing awareness of greenhouse gases are incentivizing the exploitation of renewable energy sources (RESes), in particular sun and wind, as alternatives to fossil fuels in electrical energy generation, as reported by the International Energy Agency (IEA) in Reference [1]. Such RESes are employed not only in bulk generation facilities, but they are widely embedded in distribution networks. Especially at the low voltage (LV) level, several incentivizing policies have been applied in terms of economic facilitators (such as feed-in tariffs and net-metering), resulting in a wide installation of rooftop photovoltaic (PV) units in residential areas.

Nevertheless, PV generation and electricity consumption have different daily trends and their mismatch entails the need to export a significant part of the locally-generated energy to the grid. In addition, the same amount of energy is drawn for local consumption in other time periods [2]. This practice causes inefficiency and raises several issues concerning the distribution network management (e.g., voltage regulation, congestion management, distribution power losses, etc.). At the same time, the unit price paid by the end-user for purchasing electricity is commonly higher than

the unit income obtainable by injecting energy into the grid. Since a large reduction of net-metering advantages is expected in the near future, the maximization of the self-consumption rate of the generated energy is a key point to increase the economic potential of PV. In Reference [3], storage units coupled with PV systems are analyzed in terms of profitability to make PV economically attractive even in the absence of regulatory support, taking into account the different components of costs and revenues.

Electrochemical battery energy storage systems (BESSes) are a promising solution for the maximization of customers' self-consumption, since they are nowadays available on the market for residential use, and their cost is expected to significantly decrease thanks to the spread of several technologies integrating storage devices (e.g., electric vehicles).

The aim of today's batteries, i.e., the self-consumption of the PV production, is achieved through the energy-on-demand function. In fact, if no communication systems with the distribution system operator (DSO) are available, different strategies to combine local generators and storage devices have been addressed. For instance, in Reference [4], a control strategy is presented for a residential BESS able to maximize the self-consumption and to minimize the curtailment losses caused by feed-in thresholds without need of generation/load forecasts. Results show that the increase of self-consumption is desirable from a network management perspective, given the reduction in the curtailment losses. Furthermore, the authors point out that the aggregation of several local units is preferable in comparison with district storage. In Reference [5], a comparison among a few battery discharge strategies for a grid connected building is presented, focusing on the self-consumption maximization, the time-shift function based on the predicted load, and the economic income. Neural networks are employed to set the sizing equations of the storage units, then the proposed discharge algorithms aim either at pursuing a network global optimum or the maximum user income. Analogously, in Reference [6], the authors described the design of a lithium-ion storage system to increase the matching between generation and consumption in a residential zero-energy building, resulting in a reduction of the power exchange with the grid by more than 75% and a decrease in the energy bill of 87%.

Nevertheless, several smart pricing models have been investigated. It seems to be an opportunity for DSOs to involve active end-users (integrating local generation and BESSes) in the electric system management, e.g., in the network power flow reduction [7,8] or in the voltage regulation [9]. In Reference [7], active demand is coupled with storage, improving the self-consumption in order to study the relation between annual energy flows and the storage size. Regarding innovation in the energy market, an alternative pricing strategy is proposed to incentivize the energy independency of end-users from the grid in Reference [8], whereas a network controller based on local price signals is presented in Reference [9]. Many research works are based on the demand-side management (DSM) approach, in which customers are economically remunerated for adjusting two-way power flow at their point of delivery (PoD), either in terms of absorption or injection, to contribute to congestion reduction when the distribution network is under stress. In References [10,11], some of the most common DSM approaches available in literature are surveyed to compare individual vs. cooperative management, deterministic vs. stochastic methods, and day-ahead vs. real-time operation. In Reference [12], an optimized home energy management system facilitating the RESes exploitation and the participation to DSM activities is implemented considering an optimized scheduling of the home appliances according with a varying energy price. The simultaneous optimization of both electric and gas distribution networks through DSM is investigated in Reference [13], showing a reduction of the energy bill by 20%. Generally, the DSM is achieved through both the optimized management of storage units (with scheduling procedures and real-time corrections [14]) and the classification of loads depending on their supply priority [15]. In Reference [14], the energy production, including the BESS management, is scheduled one day ahead, following which a real-time control scheme tracks the expected profile to minimize the power curtailment. A fast-balancing service for the power system is obtained through the management of controllable loads (either passive or active) in Reference [15]. The end-user satisfaction (i.e., the reduction of the inconvenience due to the scheduled loads operation)

is additionally considered in the DSM scheme proposed in Reference [16], elaborating an optimal compromise between user-budget and satisfaction, whereas these factors are used in a multi-objective optimization in Reference [17] to reduce the energy exchange with the grid and, eventually, the bill cost.

At the same time, a further income can be obtained by allowing distributed resources to participate to the ancillary services market, such as the network voltage regulation and the containment of voltage unbalances. In Reference [18], a study about the optimal sizing, siting, and managing of storage units is presented to investigate their impact on the ancillary services provision. A voltage unbalance mitigation strategy is proposed for three-phase inverters in Reference [19], aiming at the compensation of negative and zero sequence voltage components in LV systems, whereas the same approach is extended to RESes connected to medium voltage (MV) networks in Reference [20]. The exploitation of BESSes has been proposed for power quality improvement. Control schemes for reducing the harmonic distortion, both referring to a single customer equipped with a PV plant [21] and aggregating the storage contributions in a smart community [22], are discussed in the literature. The use of RESes in the dynamic grid support is highlighted in Reference [23] according to the most recent standard requirements, whereas the BESS role in stand-alone systems with wind generation is investigated in Reference [24]. Storage units are included in the management strategy of an islanded network in Reference [25]. Nevertheless, the increasing diffusion of storage systems, although compliant with European standards and national grid codes (e.g., [26,27]), may lead to safety issues. In the case of faults, portions of the LV network may be maintained energized by dispersed generators and BESSes, since their stabilizing contributions mask voltage and frequency perturbations, resulting in the failure of present passive anti-islanding protections [28,29].

An increased attention on storage systems has been recorded in the last couple of years. New norms and standards currently regulate the procedures/rules for installing and operating BESSes, both in LV distribution systems [26,27] and in MV networks (e.g., [30,31]). The main drivers of this possible market evolution are linked to:

- Avoiding the local emission of greenhouse gases (making use of full-electric appliances and decarbonized generation sources);
- Increasing self-consumption;
- Reducing the influence of electricity market variations on the customer's bill by limiting the amount of purchased energy; and
- Necessity of avoiding long power outages in the case of serious network events (very frequent in many countries) and supplying energy if the network is not yet present (rural electrification).

The BESS installation is usually considered a private investment and its economic standpoint has to be suitably accounted. This issue is discussed in several research papers. For instance, in Reference [32], it is demonstrated that a storage system may not be profitable for the customer in comparison to the case without BESS. Differently, the BESS investment is considered an interesting perspective in Reference [33], where the storage management for economically optimizing the BESS installation is addressed, taking into account the non-normal distribution of local generation and demand. Nevertheless, it should be considered that: (i) incentivizing policies are currently applied in several countries (e.g., a 50% discount in the form of tax reduction, refunded in 10 years, in the Italian context [8]); (ii) the BESS market is rapidly evolving, i.e., a significant drop in battery prices is expected as a consequence of the market volume increase; and (iii) the electricity pricing structure, e.g., energy constant price (ECP), time of use (TOU), or real-time pricing (RTP), significantly impacts on the end-user bill. In Reference [34], a general method for the components design of a PV-BESS integrated system according to a comprehensive techno-economic analysis is presented, taking into account the state-of-the-art. A cost analysis is reported in Reference [35], focusing on the residential context and considering several parameters, such as battery end-of-life criterion, battery aging behavior, electricity price, and investment costs. Outcomes of this work suggest that the 'battery parity' is possible in the next few years.

An integrated design is required for modern PV-BESS systems, which have the role of suitably managing the power flow of the active customer, e.g., (i) to optimize the generation, i.e., performing the maximum power point (MPP) tracking for maximizing the PV power output; (ii) to interact with the batteries, which are suggested to be locally sited to minimize the cable length; (iii) to supply the end-user internal loads, eventually classifying them as primary and secondary appliances in the case of an intentional islanded operation; and (iv) to exchange power surplus and deficit with the public network, eventually according to market signal or ancillary services requests from the DSO in the near future. Active end-users equipped with modern PV-BESS integrated systems could also aggregate their behaviors, according to each operating state and local available resources, to interact with the power system as an equivalent subject, able to both operate in the energy market and provide the better technical-economic results to all its participants. It should be remembered that storage systems presently available on the market are required to be compliant with the test protocols described by local grid codes, e.g., the connection standard CEI 0-21 for active customers interfaced with Italian LV public networks [27].

Currently, the majority of the commercially-available storage solutions to integrate PV systems in the residential sector consist of lithium-ion (Li-ion) batteries. Nevertheless, several technologies with different properties are worth investigating. For instance, in Reference [36], lead-acid (Pb-acid), sodium-nickel chloride ($NaNiCl_2$), Li-ion, and nickel/cadmium (NiCd) batteries are introduced, whereas a comparison based on energy, environmental, technical, and economic criteria is reported in Reference [37]. The suitability of these technologies in the residential context is addressed in Reference [38].

In this paper, the $NaNiCl_2$ battery, also known as ZEBRA in the past (acronym of Zero Emission Battery Research Activities), is considered. The high lifetime, the high peak power capacity, and reduced long-term specific cost are promising aspects, as well as the ongoing research progress. On the other hand, this technology makes use of a dedicated electrochemistry, with beta alumina as a sodium ion conducting solid electrolyte. As a consequence, the optimal performances are obtained in the temperature range 260/320 °C, i.e., 533/593 K [39,40]. Thus, the battery temperature has to be regulated through an internal heater and an external fan (the latter only in case a heavy discharging power is required, e.g., when the battery is used in electrical vehicles, during the acceleration phase or while climbing uphill).

The evolution of $NaNiCl_2$ technology is detailed with a specific focus on the residential level, where the distributed generation (DG) is mainly photovoltaic. A simplified thermoelectric analysis characterizing the management issues related to this battery and estimating the yearly economic profitability (including heating costs) is presented in this paper. Results are evaluated starting from real profiles of both load consumption and solar radiation, obtained with a quarter-hour time resolution through field measurements on an annual period. The presently-applied electricity tariffs (as defined by the Italian energy authority with reference to the third quarter of 2017) are considered.

In the following, Section 2 describes the main $NaNiCl_2$ battery advantages and recent developments in residential applications, whereas Section 3 details the presented procedure for the simplified technical-economic characterization of an active end-user equipped with a PV plant and a $NaNiCl_2$-based BESS. In Section 4, the present policies for pricing both purchased and sold electricity amounts are detailed. Section 5 reports the main results obtained from the developed algorithm and Section 6 summarizes the main conclusions. Table 1 reports all the acronyms used in the paper.

**Table 1.** List of acronyms defined in the paper, in alphabetic order.

| Acronym | Extended Meaning | Acronym | Extended Meaning |
|---|---|---|---|
| BESS | Battery energy storage system | MPP | Maximum power point |
| BMS | Battery management system | MV | Medium voltage |
| BoS | Balance of system | PoD | Point of delivery |
| CEI | Comitato Elettrotecnico Italiano | PV | Photovoltaic |
| DG | Distributed generation | SoC | State of charge |
| DSM | Demand side management | STC | Standard test condition |
| DSO | Distribution system operator | RES | Renewable energy source |
| DoD | Depth of discharge | RTP | Real time pricing |
| ECP | Energy constant price | TOU | Time of use |
| IEA | International energy agency | V2G | Vehicle-to-grid |
| LV | Low voltage | ZEBRA | Zero emission battery research activities |

## 2. $NaNiCl_2$ Battery Pros for Residential Applications

The operating principle, performance, charging/discharging curves, production process, and possible applications of sodium-nickel chloride batteries are deeply described in References [39,40]. Several successful applications of this technology in electric mobility, both considering full-electric vehicles and hybrid solutions (in which the battery is used to optimize the overall efficiency of vehicles equipped with fossil-fuel motors) are detailed in the literature. For example, in Reference [41], preliminary results obtained in the experimental field test of the Bologna's bus fleet are presented and discussed. ZEBRA batteries are also considered for the electrification of urban commercial vehicles (e.g., vans for city logistics) in the laboratory test bench described in Reference [42]. A research study [43] investigates the advantages of coupling the $NaNiCl_2$ battery with a supercapacitor to increase the dynamic and energetic performances, i.e., the power exchange between the electric drive and the overall storage system during both the acceleration phase and the regenerative electric braking. In Reference [44], according to the vehicle-to-grid (V2G) approach, the authors analyze the positive interactions between electrical vehicles and the power grid, comparing a wide range of possible storage technologies.

The features of this technology can prove very interesting in critical backup power applications (as an uninterruptible power supply). A stationary application in South California demonstrates that ZEBRA battery performances are independent of ambient temperature, self-discharge is negligible, and the heater consumption for the internal temperature regulation is low and slightly influenced by external conditions [45]. Finally, marine, submarine, and train applications are under study.

A few studies regarding the installation of ZEBRA batteries at the customer level make use of simplified battery models. In References [46,47], batteries are considered for supplying demand response (DR) and tariff arbitrage at the residential level in the United States context, whereas they are used in combination with a medium-sized PV plant to increase the self-sufficiency of a multi-apartment building in Sweden in Reference [48]. Unfortunately, this study makes use of hourly average profiles in the north of Europe and the thermal behavior of the sodium-nickel chloride batteries is not modeled in detail.

In this paper, the use of the $NaNiCl_2$ battery technology in the domestic context is considered. In particular, the integration with a local PV unit for increasing the customer self-consumption and to indirectly reduce the end-user impact on the network management (since reducing the exchanged power with the network generally means reduced voltage regulation problems and lower distribution losses) is deeply investigated by adopting a simplified thermoelectric model of the sodium-nickel chloride battery. This technology, covering a typical consumption range of some hours, shows some specific and useful performances for this specific usage:

- Highly safe operation, demonstrated by the achievement of some important certifications (according to standards UL1973 "Standard for batteries for use in light electric rail applications

and stationary applications", network equipment building standard NEBS level 3, and CE, which is the manufacturer's declaration of product's conformity with health, safety, and environmental protection standards for products sold within the European economic area). Positive results to some abuse tests, such as crash tests (i.e., forcing an operative battery against a pole with speed 50 km/h), vibration test, over-charge test, over-discharge test, short-circuit operation, submersion test, and fire exposure, are demonstrated [49]. In detail, since the battery is compliant with requirements for the vehicle use, it passes all the mentioned tests thanks to its four-barrier safety concept: barrier by the chemistry, barrier by the cell case, barrier by the thermal enclosure and barrier by the battery controller [40];

- Zero ambient emission, i.e., the storage system can be installed in a sealed environment;
- No ancillary equipment needed (e.g., air conditioners), making easier the installation;
- Full recyclability, without extra costs for the end-users thanks to a well-set recycling process, which is certificated and cost effective [40];
- Maintenance-free design;
- Wide operating temperature range without any performance de-rating (environmental temperature constraints −40/+60 °C, i.e., 233/333 K, derive exclusively from the power electronic admitted conditions), suitable for all typical location within building technical room;
- Battery partial availability in case of single cell outage to ensure anytime, as much as possible, the high level of performance. In detail, in the case the beta alumina ceramic separator breaks, a chemical reaction producing aluminum and common kitchen salt (NaCl) starts, so the aluminum shorts the current path between plus and minus and the cell resistance is suitably reduced [40]; and
- Long calendar life (15 years) and cycle life (at least 4500 cycles @ 80% depth of discharge, DoD).

Many products based on Lead-acid or lithium-ion batteries available on the market do not show the same versatile functionalities. On the other hand, the sodium technology requires energy absorption to compensate for thermal dissipation to the environment. This issue involves to suitably design both the storage system rated energy and the BESS architecture to avoid long stand-by periods, since the sodium-based technologies provide the best performances if the battery is kept constantly in operation, as better discussed and modeled in the following sections.

The battery design chosen for the residential product is based on a 48 V module. A dedicated firmware has been developed to optimally match the specific residential requirements, such as:

- Real-time current reversibility (no delay in state transition from discharge to charge and vice versa);
- Specific algorithm to allow an optimized battery heater management even in case of reduced RES generation and off grid operation;
- Suitable ModBus registers to allow a flexible remote monitoring;
- Dedicated warnings to allow a better integration at system level with electronic converters; and
- Modular design in order to allow further system capacity expansions.

In the BESS, a human-machine interface is recommended for the purpose of allowing the end-user to operate in front of the system, although apps for mobile devices are available to simplify the monitoring and the interaction with the overall system. The customer choice could range between different operative modes, such as: (i) on-grid (the battery is used to maximize the end-user self-consumption); (ii) off-grid, with automatic commutation between the grid-connected operation and the islanded condition according to local frequency/voltage measures; (iii) owned-grid (typical of rural areas not supplied by public networks, where some units could create a local micro-grid as a first electrification solution); and (iv) bypass mode (the storage system is excluded for whatever reason). In general, all the battery functions, set parameters, and local measures could be available remotely if a web server is connected to the system, for the purposes of data logging and customer support.

The $NaNiCl_2$ storage technology is continuing its evolution with the aim of both preserving the technology peculiarities and reducing the required operating temperature. For example,

in Reference [50], the operation of an improved ZEBRA battery operating at 175 °C is investigated to lower heating costs. Furthermore, in Reference [51], the authors propose the improvement of the $NaNiCl_2$ cell cycle performance through the encapsulation of Ni particles with a $Ni_3S_2$ layer, whereas in Reference [52], the thermal integration of the $NaNiCl_2$ battery with a solid oxide fuel cell prime mover is introduced to increase the overall efficiency in a residential building application.

## 3. BESS Operation Model

In this section, the algorithm characterizing the end-user operation is detailed. The procedure describes the operation of an active end-user, equipped with a PV generator and a storage system. However, the same results referred to the passive scenario or considering the sole PV unit are obtainable by nullifying the rated sizes of the PV unit and/or the BESS. The entire procedure has been implemented in Matlab® simulation software, version R2015b (MathWorks, Natick, MA, USA).

Since the PV generation is concentrated in the central hours of the day, whereas during working days the load consumption is higher in the morning and especially in the evening (e.g., considering a household owned by a couple of employees), the BESS is considered connected on the DC side of the main inverter, as depicted in Figure 1. In this way, the diurnal PV surplus is directly storable in the batteries, without requiring a double DC/AC conversion, impacting system losses. Obviously, it should be considered that PV panels are representable as current sources (with imposed current depending on the incident solar radiation) and their MPP is obtained by imposing variable voltage at their ends depending on environmental conditions (i.e., solar radiation and air temperature affecting the PV cell temperature). On the other hand, the battery no-load voltage strongly depends on the internal state of charge (SoC), whereas the operating voltage is influenced by the charging/discharging current, as a result of Ohm's law considering the batteries' equivalent internal resistance. As a consequence, the main DC/AC converter is equipped with the MPP tracking function, whereas a DC/DC converter is introduced to suitably couple the BESS to the DC bus where PV panels are connected.

Figure 1 also reports the parameters introduced in the procedure described below. For the sake of clarity, they are grouped close to the physical elements they refer to, whereas their meaning is described in the following explanation of the developed algorithm. Power flows are reported with bold red font. All the variables and parameters are listed in Table 2, with indications of the mathematical expressions in which they first appear.

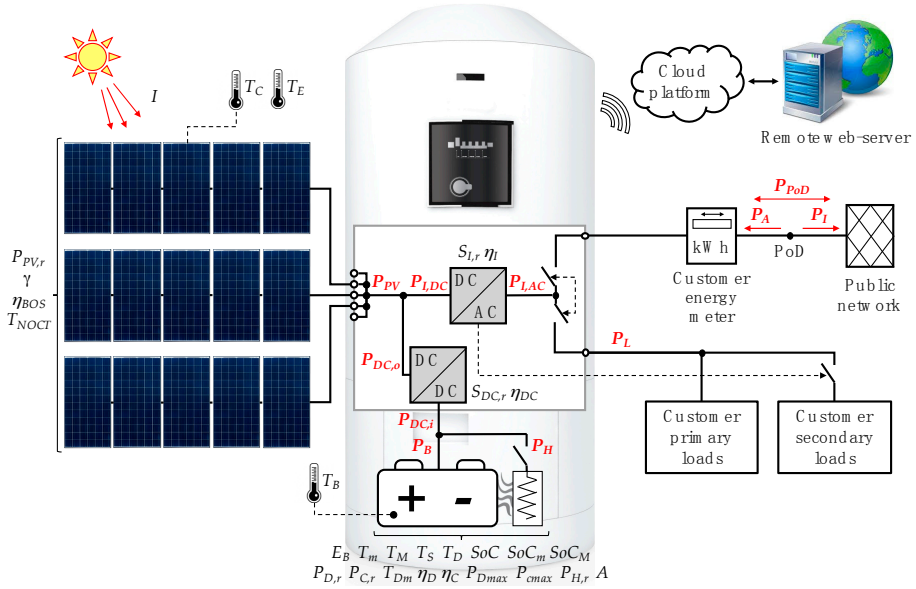


**Figure 1.** Electrical scheme depicting the represented model.

**Table 2.** List of variables and parameters, with indications of the mathematical expressions in which they first appear.

| Variable and Parameter | Symbol | Unit of Measure | Mathematical Expression |
|---|---|---|---|
| Generic time instant | $t$ | s | (1) |
| Duration of the elementary time interval | $\Delta t$ | s | (1) |
| PV power injected in the DC bus | $P_{PV}$ | kW | (1) |
| PV plant rated power | $P_{PV,r}$ | kW | (1) |
| Effective solar irradiance | $I$ | W/m$^2$ | (1) |
| Solar irradiance in STC | $I_{STC}$ | W/m$^2$ | (1) |
| Temperature efficiency of PV cells | $\eta_T$ | dimensionless | (1) |
| BoS equivalent efficiency | $\eta_{BOS}$ | dimensionless | (1) |
| Thermal loss coefficient of PV cells | $\gamma$ | 1/°C | (2) |
| PV cells temperature | $T_C$ | °C | (2) |
| PV cells temperature in STC | $T_{STC}$ | °C | (2) |
| Air temperature where the PV plant is installed | $T_E$ | °C | (3) |
| Normal operating cell temperature of PV cells | $T_{NOCT}$ | °C | (3) |
| Interpolated AC/DC converter efficiency as a function of the effective loading rate | $\eta_I$ | dimensionless | (4) |
| Linearization of AC/DC converter efficiency, constant value | $a$ | dimensionless | (4) |
| Linearization of AC/DC converter efficiency, slope | $b$ | dimensionless | (4) |
| AC/DC converter DC power | $P_{I,DC}$ | kW | (4) |
| AC/DC converter rated power | $S_{I,r}$ | kVA | (4) |
| AC/DC converter efficiencies at standard loading rates | $\eta_{INV}$ | dimensionless | (4) |
| Standard loading rates for characterizing the AC/DC converter efficiency | $p$ | dimensionless | (4) |
| Power exchange with the public network | $P_{PoD}$ | kW | (5) |
| AC/DC converter AC power | $P_{I,AC}$ | kW | (5) |
| Load absorption | $P_L$ | kW | (5) |
| Injected power at the PoD | $P_I$ | kW | (6) |
| Absorbed power at the PoD | $P_A$ | kW | (7) |
| Injected energy at the PoD | $E_I$ | kWh | (8) |
| Overall time duration of the analysis | $T$ | s | (8) |
| Absorbed energy at the PoD | $E_A$ | kWh | (9) |
| Effective hourly decrease in the battery internal temperature | $T_D$ | °C | (10) |
| Battery hourly cooling rate starting from 300 °C | $T_S$ | °C | (10) |
| Battery internal temperature | $T_B$ | °C | (10) |
| Maximum discharging power | $P_{Dmax}$ | kW | (11) |
| Rated discharging power | $P_{D,r}$ | kW | (11) |
| Battery State of Charge | $SoC$ | dimensionless | (11) |
| Minimum admitted State of Charge | $SoC_m$ | dimensionless | (11) |
| Battery efficiency during the discharging phase | $\eta_D$ | dimensionless | (11) |
| Storable energy in rated conditions | $E_B$ | kWh | (11) |
| DC/DC converter rated power | $S_{DC,r}$ | kW | (11) |
| Minimum admitted discharging time duration for preventing battery internal over-temperature | $T_{Dm}$ | °C | (11) |
| Maximum charging power | $P_{Cmax}$ | kW | (12) |
| Rated charging power | $P_{C,r}$ | kW | (12) |
| Maximum admitted State of Charge | $SoC_M$ | dimensionless | (12) |
| Battery efficiency during the charging phase | $\eta_C$ | dimensionless | (12) |
| Target for the AC/DC converter AC power | $P_{I,AC}$* | kW | (13) |
| Target for the AC/DC converter DC power | $P_{I,DC}$* | kW | (14) |
| Target for the DC/DC converter output power | $P_{DC,o}$* | kW | (15) |
| Target for the DC/DC converter input power | $P_{DC,i}$* | kW | (16) |
| Interpolated DC/DC converter efficiency as a function of the effective loading rate | $\eta_{DC}$ | dimensionless | (16) |
| DC/DC converter rated power | $S_{DC,r}$ | kW | (16) |
| Effective heater power absorption | $P_H$ | kW | (17) |
| Battery heater rated power | $P_{H,r}$ | kW | (17) |
| Minimum admitted internal temperature | $T_m$ | °C | (17) |
| Required battery power | $P_B$* | kW | (18) |
| Effective battery power | $P_B$ | kW | (19) |
| Effective DC/DC converter input power | $P_{DC,i}$ | kW | (20) |
| Effective DC/DC converter output power | $P_{DC,o}$ | kW | (21) |
| Effective AC/DC converter DC power | $P_{I,DC}$ | kW | (22) |
| Maximum power absorption at the PoD | $P_{A,max}$ | kW | (25) |
| End-user contractual power | $P_{bill}$ | kW | (26) |
| Maximum power injection at the PoD | $P_{I,max}$ | kW | (27) |
| Self-sufficiency ratio | $SSR$ | dimensionless | (28) |
| Self-consumption ratio | $SCR$ | dimensionless | (29) |
| Heater energy consumption | $E_H$ | kWh | (30) |
| Battery aging | $A$ | cycles | (31) |
| Average variation of power exchange at the PoD between subsequent time instants | $\Delta P_{PoD}$ | kW | (32) |
| Number of elementary time intervals | $N$ | dimensionless | (32) |

**Table 2.** *Cont.*

| Variable and Parameter | Symbol | Unit of Measure | Mathematical Expression |
|---|---|---|---|
| Overall customer bill | $C$ | €/year | (33) |
| Bill component due to electricity consumption | $C_E$ | €/year | (33) |
| Bill component due to electricity transportation and meters management | $C_{TR}$ | €/year | (33) |
| Bill component due to overall system costs coverage | $C_S$ | €/year | (33) |
| Bill component due to excise duty | $C_{EX}$ | €/year | (33) |
| Bill component due to value-added tax | $VAT$ | €/year | (33) |
| Value-added tax rate | $v$ | dimensionless | (33) |
| Fixed component of $C_E$ | $C_{E,0}$ | €/month | (34) |
| Variable component of $C_E$, overall cost | $C_{E,E}$ | €/year | (34) |
| Variable component of $C_E$, unit cost in peak hours | $c_{E,E1}$ | €/kWh | (35) |
| Variable component of $C_E$, unit cost in off-peak hours | $c_{E,E2}$ | €/kWh | (35) |
| Absorbed energy at the PoD in peak hours | $E_{A1}$ | kWh | (35) |
| Absorbed energy at the PoD in off-peak hours | $E_{A2}$ | kWh | (35) |
| Variable component of $C_E$, dispatching cost | $C_{E,D}$ | €/year | (35) |
| $C_{E,D}$, unit cost applied to the first energy bracket | $c_{E,D1}$ | €/kWh | (36) |
| First energy bracket of $E_A$ | $E_1$ | kWh | (36) |
| $C_{E,D}$, unit cost applied to the second energy bracket | $c_{E,D2}$ | €/kWh | (36) |
| Second energy bracket of $E_A$ | $E_2$ | kWh | (36) |
| $C_{E,D}$, unit cost applied to the third energy bracket | $c_{E,D3}$ | €/kWh | (36) |
| Third energy bracket of $E_A$ | $E_3$ | kWh | (36) |
| $C_{E,D}$, unit cost applied to the fourth energy bracket | $c_{E,D4}$ | €/kWh | (36) |
| Fourth energy bracket of $E_A$ | $E_4$ | kWh | (36) |
| Fixed component of $C_{TR}$ | $C_{TR,0}$ | €/month | (37) |
| Power component of $C_{TR}$ | $C_{TR,P}$ | €/month | (37) |
| Energy component of $C_{TR}$ | $C_{TR,E}$ | €/year | (37) |
| Power component of $C_{TR}$, unit cost | $c_{TR,P}$ | €/(kW month) | (37) |
| Energy component of $C_{TR}$, unit cost | $c_{TR,E}$ | €/kWh | (37) |
| Bill component due to excise duty, unit cost | $c_{EX}$ | €/kWh | (38) |
| Part of the customer consumption charged by $c_{EX}$ | $E_A$ * | kWh | (38) |
| Bill component due to excise duty, first energy threshold | $E_{Ae1}$ | kWh | (38) |
| Bill component due to excise duty, second energy threshold | $E_{Ae2}$ | kWh | (38) |
| Revenue of injected energy at the PoD | $R_I$ | €/year | (39) |
| Energy selling price | $r_I$ | €/kWh | (39) |

### *3.1. PV Unit*

At the time instant $t$, the PV unit makes the power $P_{PV}(t)$ available on the DC bus, evaluated as in Equation (1), where $I(t)$ (W/m$^2$) is the mean solar irradiance on the PV surface in the $t$-th elementary time interval $\Delta t$ (s), $I_{STC}$ is the same parameter as in the standard test conditions (STCs, solar irradiance 1000 W/m$^2$, cell temperature 25 °C, and solar spectrum AM 1.5), and $P_{PV,r}$ (W) is the PV unit rated power.

$$P_{PV}(t) = P_{PV,r}\,\frac{I(t)}{I_{STC}}\,\eta_T(t)\,\eta_{BOS} \tag{1}$$

Remembering that the rated characteristics of PV panels refer to STCs, the thermal losses in the case where the PV cell temperature differs from the standard value (25 °C) are represented as equivalent efficiency $\eta_T(t)$ (dimensionless) defined as in Equation (2), where $\gamma < 0$ (1/°C) is the thermal losses coefficient, commonly made available in the PV panel datasheet, $T_C(t)$ is the PV cell temperature at the time instant $t$, and $T_{STC}$ is 25 °C. All the other losses affecting the PV generation up to the DC stage of the AC/DC converter, generally named as balance of system (BoS) losses (e.g., mismatching, pollution, reflection, ohmic losses on DC cables, etc.), are grouped in the equivalent efficiency $\eta_{BOS}$ (dimensionless):

$$\eta_T(t) = 1 + \gamma\,(T_C(t) - T_{STC}) \tag{2}$$

In the case where $T_C(t)$ is not available from field measurements, it could be estimated as in Equation (3), considering the corresponding environmental temperature $T_E(t)$ and the PV panel

nominal operating cell temperature $T_{NOCT}$ (°C), directly dependent on the PV technology and usually reported in the PV panels datasheets.

$$T_C(t) = T_E(t) \frac{I(t)}{800 \left[\frac{W}{m^2}\right]} (T_{NOCT} - 20\ [^\circ C]) \tag{3}$$

### 3.2. End-User Operation without BESS

Without a BESS, the inverter converts the entire PV production to the AC bus, i.e., the power flow $P_{I,DC}(t)$ is equal to $P_{PV}(t)$. The DC/AC conversion efficiency is obtained from PV inverter datasheets. Weighted values are usually available, e.g., the European efficiency and the California Energy Commission efficiency, which provide differently weighted converter efficiencies at several loadings. Nevertheless, aiming at better representing the power converter operation and losses, the procedure supposes to know the inverter efficiency curve as a series of $i$-th couples $p(i) - \eta_{INV}(i)$, where $p(i)$ are several machine loading rates and $\eta_{INV}(i)$ are the corresponding conversion efficiencies. Thus, the considered converter efficiency $\eta_I(t)$ depending on the effective loading $P_{I,DC}(t)/S_{I,r}$ is linearly interpolated as in Equation (4):

$$\begin{cases} \eta_I(t) = a(t) + b(t) \frac{P_{I,DC}(t)}{S_{I,r}} \\ b(t) = \frac{\eta_{INV}(i+1) - \eta_{INV}(i)}{p(i+1) - p(i)} \\ a(t) = \eta_{INV}(i) - b\ p(i) \end{cases} \quad where\ p(i) < \frac{P_{I,DC}(t)}{S_{I,r}} \leq p(i+1) \tag{4}$$

The end-user's loads absorb the power $P_L(t)$ at the time instant $t$, thus, in the case where the PV generation overcomes the local consumption, the PV surplus is injected into the grid. Considering the sole PV unit, the power exchanged with the network at the PoD $P_{PoD}(t)$ is, thus, computed with Equation (5) and the result is positive in the case of power exported to the public network (generator convention). The injected power flow $P_I(t)$ and the absorbed power flow $P_A(t)$ are defined as in Equations (6) and (7), respectively:

$$P_{PoD}(t) = P_{I,AC}(t) - P_L(t) = P_{I,DC}(t)\ \eta_I(t) - P_L(t) \tag{5}$$

$$\begin{cases} P_I(t) = P_{PoD}(t)\ if\ P_{PoD}(t) \geq 0 \\ P_I(t) = 0\ if\ P_{PoD}(t) < 0 \end{cases} \tag{6}$$

$$\begin{cases} P_A(t) = 0\ if\ P_{PoD}(t) \geq 0 \\ P_A(t) = P_{PoD}(t)\ if\ P_{PoD}(t) < 0 \end{cases} \tag{7}$$

In a long-term analysis with time duration $T$ (where $T$ is usually assumed to be equal to one year to suitably consider both the load and the generation seasonal variations), the end-user injects into the network the energy amount $E_I$ and absorbs from the distribution system the energy amount $E_A$, defined as in Equations (8) and (9), respectively. These parameters will be used for the economic comparison between different scenarios, according to the adopted schemes for pricing purchased and sold energies (detailed in the following):

$$E_I = \sum_{t \in T} P_I(t)\ \Delta t \tag{8}$$

$$E_A = -\sum_{t \in T} P_A(t)\ \Delta t \tag{9}$$

### 3.3. BESS Model

In this procedure, the BESS is considered an end-user's investment and no local ancillary service markets are established. The storage unit is managed with the aim of optimizing the final customer's self-consumption and its economic profitability. Consequently, the BESS is charged in the case where the solar availability surpasses the local load consumption, and then it is discharged to reduce the amount of energy purchased from the public network when the generation is insufficient or absent.

The developed BESS model takes into account the peculiarities of the $NaNiCl_2$ technology, focused on the management of its internal temperature $T_B(t)$, which is required to be maintained in the admitted range ($T_m/T_M$) (°C). In particular, the upper temperature threshold is one of the constraints during the discharging phase, considering that $T_B(t)$ significantly increases in the case of fast discharges [42]. Different from use in electrical vehicles, and considering real domestic load trends, $NaNiCl_2$ batteries for stationary applications are not equipped with cooling fans to improve the thermal insulation of the battery, i.e., to reduce the heater consumption in order to maintain the internal temperature $T_B$ in the admitted range. Thus, the constraint $T_M$ could limit the discharging power, as detailed in the following. Figure 2a represents field measurements collected by means of laboratory tests to characterize the temperature behavior, depending on the considered discharging regime: the battery (suitable for residential applications in terms of storable energy, rated voltages, and sizes) is completely discharged with different time durations, obtaining consequent increases in the internal temperature.

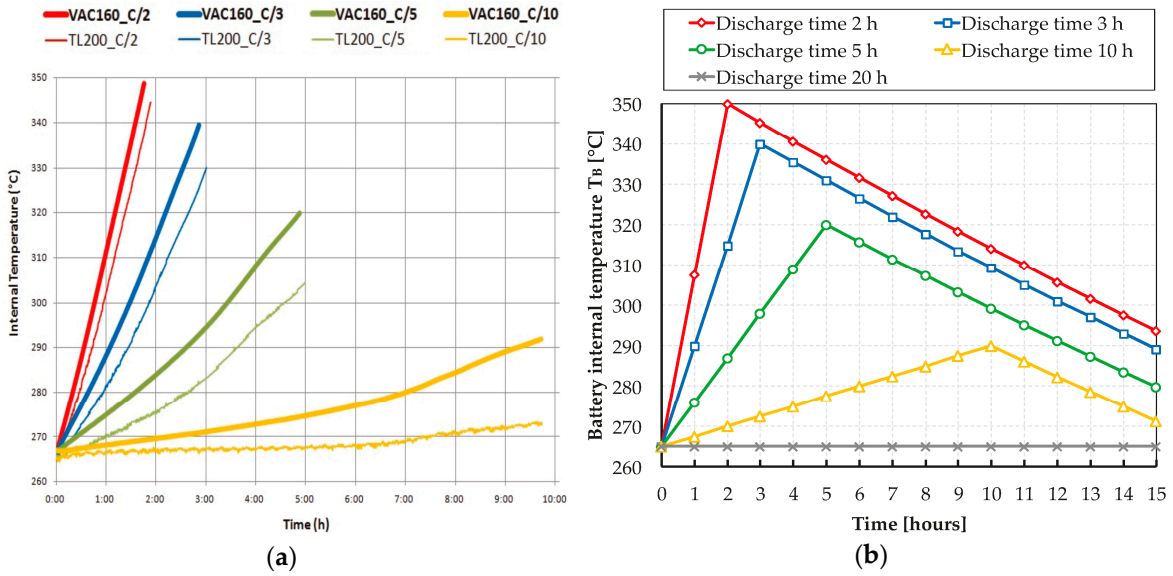


**Figure 2.** Thermal characterization of $NaNiCl_2$ batteries for residential applications. (**a**) Battery technical specifications, resulting from laboratory measurements of the time trends of the internal temperature $T_B$ with different discharging rates (2 h, 3 h, 5 h, and 10 h) for a couple of commercially-available battery models (VAC160, bold lines, and TL200); (**b**) Equivalent model for the representation of the thermal behavior of the studied battery model VAC160, for different discharging rates (in this picture, the horizontal axis is extended to 15 h to partially depict the cooling processes once the discharging phases end).

After the complete discharge of the battery, it is left in the stand-by condition, which results in the battery cooling, represented through the temperature decrease $T_D(t)$ (°C) in the time interval $\Delta t$, as evaluated by Equation (10). In the model, $T_D(t)$ depends on the internal temperature $T_B(t)$ in comparison with the standard environmental temperature of 20 °C, whereas $T_S$ (°C/h) is the hourly reduction in the internal temperature when it starts from 300 °C. Figure 2b reports the equivalent representation adopted in this paper, as summarized in Table 3. It is important to note that the model is very accurate, since only negligible errors are introduced in characterizing the thermal management

of the battery. Intermediate discharging conditions are modeled by linearizing the behavior between adjacent discharging trends, similar to Equation (4).

$$T_D(t) = T_S \frac{T_B(t) - 20\ [^\circ C]}{300\ [^\circ C] - 20\ [^\circ C]}\ \Delta t \tag{10}$$

**Table 3.** Equivalent representation of the battery temperature increase depending on the discharging time duration (values are coherent with Figure 2b). In the case where the discharging time duration overpasses 20 h, the battery thermally behaves as in stand-by conditions.

| Discharging Time Duration (h) | Temperature Increase (°C) |
|---|---|
| 2 | 42.5 |
| 3 | 25 |
| 5 | 11 |
| 10 | 2.5 |
| 20 | 0 (thermal equilibrium) |
| >20 | Temperature decreases as in stand-by conditions |

Through this temperature characterization, the minimum admitted discharging time duration $T_{Dm}(t)$ (h) is computed by knowing the battery internal temperature $T_B(t)$ and the maximum admitted threshold $T_M$. Consequently, the maximum admitted discharging power $P_{Dmax}(t)$ at the $t$-th time instant is obtained as the most binding among several operational constraints, synthetically represented in Equation (11). The parameter $P_{D,r}$ is the BESS rated power in the discharging phase. The second constraint is related to the internal SoC at the $t$-th time interval $SoC(t)$, which cannot surpass the admitted thresholds $SoC_m$ (dimensionless) and $SoC_M$ (dimensionless) at the end of the time interval $\Delta t$, whereas $\eta_D$ (dimensionless) is the discharging efficiency and $E_B$ (kWh) is the storage system rated energy. The DC/DC converter rated power is called $S_{DC,r}$ (kVA).

$$P_{Dmax}(t) = min\left[P_{D,r};\ \frac{(SoC(t) - SoC_m)\ \eta_D\ E_B}{\Delta t}; S_{DC,r};\ \frac{SoC(t)\ \eta_D\ E_B}{T_{Dm}}\right] \tag{11}$$

Similarly, taking into account that the charging phase does not increment the battery internal temperature, the maximum admitted charging power $P_{Cmax}(t)$ is can be evaluated by using Equation (12), where $P_{C,r}$ is the BESS rated power in the charging phase and $\eta_C$ (dimensionless) is the charging efficiency:

$$P_{Cmax}(t) = min\left[P_{C,r};\ \frac{(SoC_M - SoC(t))\ E_B}{\eta_C\ \Delta t}; S_{DC,r}\right] \tag{12}$$

To maximize the self-consumption of the PV generation, the output of the DC/AC converter should be equal to the customer's loads overall consumption, as for the constraint of Equation (13). This means that the desired power on the DC side of the DC/AC converter $P^*_{I,DC}(t)$ can be evaluated by Equation (14). In this case, for the purpose of simplicity, which means avoiding iterative computations, the loading rate of the DC/AC converter, required to estimate the static machine efficiency, is evaluated considering the desired output power $P^*_{I,AC}(t)$, instead of $P^*_{I,DC}(t)$ as previously described in Equation (4). However, it should be noted that this simplification has negligible consequences on the overall computation, since the DC/AC converter efficiency is very high in a wide spectrum of loading rates and stand-by losses are limited to few Watts or less:

$$P^*_{I,AC}(t) = P_L(t) \tag{13}$$

$$P^*_{I,DC}(t) = \frac{P_L(t)}{\eta_I(t)} = \frac{P_L(t)}{\eta_I\left(\frac{P^*_{I,AC}(t)}{S_{I,r}}\right)} \tag{14}$$

Considering the PV generator contribution, the desired power flow on the BESS DC/DC converter, at both the output port $P^*_{DC,o}(t)$ and the input port $P^*_{DC,i}(t)$, are computed as in Equations (15) and (16), respectively. The DC/DC converter efficiency $\eta_{DC}(t)$ is characterized by Equation (4), considering the static converter estimated loading rate equal to $P^*_{DC,o}(t)/S_{DC,r}$:

$$P^*_{DC,o}(t) = P^*_{I,DC}(t) - P_{PV}(t) \tag{15}$$

$$\begin{cases} P^*_{DC,i}(t) = \frac{P^*_{DC,o}(t)}{\eta_{DC}(t)} = \frac{P^*_{DC,o}(t)}{\eta_{DC}\left(\frac{P^*_{DC,o}(t)}{S_{DC,r}}\right)} \; if \; P^*_{DC,o}(t) \geq 0 \\ P^*_{DC,i}(t) = P^*_{DC,o}(t)\eta_{DC}(t) \; = P^*_{DC,o}(t)\eta_{DC}\left(\frac{\left|P^*_{DC,o}(t)\right|}{S_{DC,r}}\right) \; if \; P^*_{DC,o}(t) < 0 \end{cases} \tag{16}$$

During the charging phases, the stand-by condition (e.g., when the batteries are no longer able to supply the end-user's load since the minimum admitted SoC has been reached) or in the case of very weak discharging (as previously reported in Table 3), if the battery internal temperature decreases close to the lower admitted threshold $T_m$, an additional heating resistance has to be switched on. This regulates the internal temperature in the permitted range, avoiding a dangerous over-cooling, i.e., to compensate the thermal losses with the external environment. When the heater is switched on, its power absorption $P_H(t)$, supplied by the battery bus, has to be considered. The heater absorption $P_H(t)$ is lightly correlated with both the internal temperature and the environmental conditions. Assuming a reference environmental temperature of 20 °C, $P_H(t)$ is estimable through Equation (17), where $P_{H,r}$ (W) is the heater rated power, absorbed to maintain the internal temperature close to 300 °C:

$$P_H(t) = P_{H,r}\frac{T_B(t) - 20\ [^\circ C]}{300\ [^\circ C] - 20\ [^\circ C]} \; if \; [T_B(t) - T_m] < T_D(t) \; in \; the \; case \; of \begin{bmatrix} charge \\ stand-by \\ weak \; discharge \end{bmatrix} \tag{17}$$

The desired battery power flow $P^*_B(t)$ is evaluated as in Equation (18). Then, the discharging and the charging power constraints $P_{Dmax}(t)$ and $P_{Cmax}(t)$ are applied and the effective power flow on the storage unit terminals $P_B(t)$ is obtained through Equation (19):

$$P^*_B(t) = P^*_{DC,i}(t) + P_H(t) \tag{18}$$

$$\begin{cases} P_B(t) = \min[P^*_B(t); P_{Dmax}(t)] \; if \; P^*_B(t) \geq 0 \\ P_B(t) = \max[P^*_B(t); -P_{Cmax}(t)] \; if \; P^*_B(t) < 0 \end{cases} \tag{19}$$

Proceeding from the battery to the main system, the effective power at the DC/DC converter input terminals is consequently obtained by means of Equation (20), and the power exchange between the BESS and the PV panel DC bus is computed using Equation (21), depending on the effective sign of the converted power. The power flow on the DC side terminals of the DC/AC converter $P_{I,DC}(t)$ is, therefore, evaluated by Equation (22):

$$P_{DC,i}(t) = P_B(t) - P_H(t) \tag{20}$$

$$\begin{cases} P_{DC,o}(t) = P_{DC,i}(t)\,\eta_{DC}(t) = P_{DC,i}(t)\,\eta_{DC}\left(\frac{P_{DC,i}(t)}{S_{DC,r}}\right) \; if \; P_{DC,i}(t) \geq 0 \\ P_{DC,o}(t) = \frac{P_{DC,i}(t)}{\eta_{DC}(t)} \; = \frac{P_{DC,i}(t)}{\eta_{DC}\left(\frac{\left|P_{DC,i}(t)\right|}{S_{DC,r}}\right)} \; if \; P_{DC,i}(t) < 0 \end{cases} \tag{21}$$

$$P_{I,DC}(t) = P_{DC,o}(t) + P_{PV}(t) \tag{22}$$

It should be noted that in the case of a BESS connected on the DC side, a bidirectional DC/AC converter has to be considered, since the thermal regulation of the battery and/or its stand-by consumption for supplying the internal battery management system (BMS) could require a small

absorption from the public network if the SoC is close to the lowest admitted value $SoC_m$ and the PV unit does not generate power (e.g., during nighttime).

The power flow made available on the AC side of the DC/AC converter $P_{I,AC}(t)$ is evaluated by Equation (4), taking into account the direction of the power flowing in the converter. Finally, Equation (5) computes the power exchange with the main network. At the end of each elementary time interval $\Delta t$, considering the 100% coulombic efficiency of $NaNiCl_2$ batteries [39,40,42], the integer parameters $SoC(t)$ and $T_B(t)$ are updated through Equations (23) and (24):

$$\begin{cases} SoC(t+1) = SoC(t) - \frac{P_B(t)\ \Delta t}{\eta_D\ E_B}\ if\ P_B(t) \geq 0 \\ SoC(t+1) = SoC(t) - \frac{P_B(t)\ \eta_C\ \Delta t}{E_B}\ if\ P_B(t) < 0 \end{cases} \quad (23)$$

$$\begin{cases} T_B(t+1) = T_B(t) - T_D(t)\ if\ P_H(t) = 0 \\ T_B(t+1) = T_B(t)\ if\ P_H(t) > 0 \end{cases} \quad (24)$$

### 3.4. Outputs of the Procedure

The operating conditions of the system in a long-term period $T$ are represented by the procedure as arrays with length $N = T/\Delta t$ (dimensionless). With the aim of summarizing and assessing the BESS advantages and its economic profitability, the following parameters are obtained as output:

- Maximum power absorption $P_{A,max}$, defined through Equation (25) and impacting the contractual power of the end-user supply $P_{bill}$ (kW) as in Equation (26), and maximum power injection $P_{I,max}$ according to Equation (27). In the Italian context, $P_{bill}$ can assume the values 3, 4.5, 6, or 10 kW. It should be noted that introducing a BESS could be a way to reduce the end-user's contractual power $P_{bill}$, thus reducing some of the components of the electricity bill.

$$P_{A,max} = max[-P_A(t)] \quad (25)$$

$$\begin{cases} P_{bill} = min[3; 4.5; 6; 10] \\ P_{bill} \geq P_{A,max} \end{cases} \quad (26)$$

$$P_{I,max} = max[P_I(t)] \quad (27)$$

- Energy absorption $E_A$ (kWh), evaluated in a long-term time period $T$ (e.g., one year). The reduction of the purchased energy is one of the BESS economic benefits. For the bill computation, the overall consumption $E_A$ is divided considering peak hours ($E_{A1}$ (kWh), from Monday to Friday, from 8 a.m. to 7 p.m. [8]) and other time periods, such as nighttime, weekends, and holidays ($E_{A2}$ (kWh)).
- Energy sold to the public network $E_I$ (kWh), i.e., one of the investment revenues according to the considered selling pricing mechanism, evaluated in a long-term time period $T$. Parameters $P_{bill}$, $E_A$, and $E_I$, computed in different scenarios (passive end-user, active end-user with the sole PV unit, and smart end-user integrating the BESS), will be used to evaluate the BESS economic advantages according to the presently-adopted schemes for pricing purchased and sold energies.
- According to Reference [48], the self-sufficiency ratio $SSR$ and the self-consumption ratio $SCR$, evaluated by Equations (28) and (29), respectively:

$$SSR = 1 - E_A / \sum_{t \in T} P_L(t)\ \Delta t \quad (28)$$

$$SCR = 1 - E_I / \sum_{t \in T} P_{PV}(t)\ \Delta t \quad (29)$$

- The battery energy consumption $E_H$ (kWh) for maintaining the internal temperature higher than the minimum threshold $T_m$. In the observation period $T$, $E_H$ is the sum of the heater consumption $P_H(t)$ multiplied by the elementary time interval $\Delta t$, as described in Equation (30):

$$E_H = \sum_{t \in T} P_H(t)\ \Delta t \tag{30}$$

- The battery aging $A$ (cycles) consequent to its operation in the time period $T$. An advanced battery lifetime prediction model is introduced in Reference [53], in which a lead-acid battery pack supplies frequent partial charging/discharging cycles. In this paper, for the purpose of simplicity and considering that the BESS operation respects all the battery constrains (e.g., admitted charging/discharging power, So C range, etc.), the effective cycle counting method is used as lifetime model [54]. Thus, the parameter $A$ is obtained through Equation (31), by considering the sole discharging phases (when $P_B(t) > 0$). However, it is important to note that partial discharges of the storage system have a very weak effect in terms of battery aging in comparison with deep discharges. Therefore, the way parameter $A$ is obtained involves a precautionary over-estimation of the battery aging, since the effective lifetime could be longer, having positive impacts on the business plan of the BESS investment.

$$A = \sum_{t \in T} \frac{\overline{P_B}(t)\ \Delta t}{E_B}\ where \begin{cases} \overline{P_B}(t) = P_B(t)\ if\ P_B(t) \geq 0 \\ \overline{P_B}(t) = 0\ if\ P_B(t) < 0 \end{cases} \tag{31}$$

- Statistical distribution of the most representative parameters, such as the power exchange $P_{PoD}$ between the end-user and the public network, the battery power contribution $P_B$, and the BESS SoC, are obtained. The minimal SoC frequency $MSF$, i.e., the relative time in which the BESS SoC is close to $SoC_m$, is computed as suggested in Reference [48]. In addition, for a deeper comprehension of the model considering the seasonal variations of both the load consumption and the PV generation, the main outputs are displayed separately for the spring-summer period (from 21 March to 21 September) and for the fall-winter phase. This analysis allows for the identification of the parameters that have the greatest influence on the overall economic interest in the BESS installation, e.g., the thermal consumption for preserving the battery internal temperature.

Finally, the average variation of the power exchange $P_{PoD}$, named as $\Delta P_{PoD}$ (kW), is evaluated for all the analyzed configurations through Equation (32) to give an immediate representation of how much the power profile is variable depending on the load behavior, combined with the solar availability and the BESS management strategy. This parameter is very interesting from the DSO's point of view, since very quick actions to regulate the network operating conditions are required in the case of a high value of $\Delta P_{PoD}$.

$$\Delta P_{PoD} = \frac{\sum_{t=2}^{N} |P_{PoD}(t) - P_{PoD}(t-1)|}{N-1} \tag{32}$$

## 4. Present Pricing Policies for Purchased and Sold Energies: The Italian Case

### *4.1. Purchased Energy*

Although if other, more complex, pricing policies are under discussion for encouraging virtuous behaviors in active end-users (e.g., [8]), considering $T$ = 1 year, the household customer bill $C$ (€/year) is evaluated through Equation (33), referring to the present Italian rules:

$$C = C_E + C_{TR} + C_S + C_{EX} + VAT = (C_E + C_{TR} + C_S + C_{EX})(1 + v) \tag{33}$$

Consequently, in all the analyzed scenarios, the cost of the yearly purchased electricity is the sum of several components, which are:

- Electricity consumption $C_E$ (€/year), which is sum of two subcomponents, as in Equation (34):

$$C_E = 12\, C_{E,0} + C_{E,E} \tag{34}$$

  - Fixed amount $C_{E,0}$ (€/month), with value depending on the type of the domestic end-user (residence house or not), as reported in Table 4;
  - Amount $C_{E,E}$ (€/year), depending on the yearly absorption $E_A$ according to Equation (35).

$$C_{E,E} = [c_{E,E1} E_{A1} + c_{E,E2} E_{A2}] + C_{E,D} \tag{35}$$

The addend reported in the first squared brackets represents the market cost of energy, as a consequence of the simplification reserved to household customers. In general, following a TOU approach, different unit prices are assigned for peak hours ($c_{E,E1}$ (€/kWh)) and off-peak periods ($c_{E,E2}$ (€/kWh)). However, the end-user has the possibility of selecting an ECP policy, i.e., a flat value $c_{E,E} = c_{E,E1} = c_{E,E2}$ (€/kWh) (not depending on the time of use of the purchased energy). The second addend $C_{E,D}$ covers the dispatching cost; it is required only for residence house customers and its unit cost $c_{E,Dx}$ (€/kWh) is assigned according to the purchased energy brackets $E_x$ (kWh/year) reported in Table 4. Thus, $C_{E,D}$ is finally evaluated as in Equation (36).

$$\begin{cases} C_{E,D} = c_{E,D1} E_A \; if \; E_A \le E_1 \\ C_{E,D} = c_{E,D1} E_1 + c_{E,D2}(E_A - E_1) \; if \; E_1 < E_A \le E_2 \\ C_{E,D} = c_{E,D1} E_1 + c_{E,D2}(E_2 - E_1) + c_{E,D3}(E_A - E_2) \; if \; E_2 < E_A \le E_3 \\ C_{E,D} = c_{E,D1} E_1 + c_{E,D2}(E_2 - E_1) + c_{E,D3}(E_3 - E_2) + c_{E,D4}(E_A - E_3) \; if \; E_A > E_3 \end{cases} \tag{36}$$

- Electricity transportation and meters management $C_{TR}$ (€/year), sum of three subcomponents as represented in Equation (37):

$$\begin{aligned} C_{TR} &= 12\, C_{TR,0} + 12\, C_{TR,P} + C_{TR,E} \\ &= 12\, C_{TR,0} + 12\, c_{TR,P}\, P_{bill} + c_{TR,E}\, E_A \end{aligned} \tag{37}$$

  - Fixed amount $C_{TR,0}$ (€/month);
  - Power component $C_{TR,P}$ (€/month), linearly dependent on the contractual power $P_{bill}$ with the unit cost $c_{TR,P}$ (€/kW month);
  - Energy component $C_{TR,E}$ (€/year), obtained by multiplying the unit cost $c_{TR,E}$ (€/kWh) by the annual energy absorption $E_A$. Although if the same energy brackets are introduced, values of $c_{TR,Ex}$ are presently unaltered with the annual purchased energy $E_A$, as demonstrated in Table 4.

- Overall system costs coverage $C_S$ (€/year), which includes several contributions applied to the electricity bill to compensate national costs (e.g., renewables incentives, nuclear plant decommissioning, policies supporting needy end-users, etc.). In particular, $C_S$ is obtained by adding a couple of contributions:

  - Fixed amount $C_{S,0}$ (€/month), required only to non-resident customers (e.g., holiday houses) as reported in Table 4;
  - Component $C_{S,E}$ (€/year), evaluated considering the unit costs $c_{S,Ex}$ (€/kWh) which vary according to the purchased energy brackets reported in Table 4, similar to Equation (34).

- Excise duty $C_{EX}$ (€/year), evaluated on the yearly energy absorption $E_A$ through the unit cost $c_{EX}$ (€/kWh). For resident customers, a complete exemption is provided in case $E_A \le E_{Ae1}$, but this

benefit is progressively withdrawn if the yearly energy purchase $E_A$ surpasses the threshold $E_{Ae2}$. Therefore, the excise duty $C_{EX}$ is computed by applying the unit excise duty $c_{EX}$ to the energy amount $E_A^*$ (kWh) defined in Equation (38). This means that a customer with a yearly energy absorption $E_A > (E_{Ae1}+E_{Ae2})$ is required to pay the excise duty on the overall consumption.

$$\begin{cases} C_{EX} = c_{EX}\, E_A^* \\ if\ resident\ customer\ E_A^* = max[0; E_A - min[E_{Ae1}; max[0;\ (E_{Ae1} + E_{Ae2} - E_A)]]] \\ if\ not\ resident\ customer\ E_A^* = E_A \end{cases} \quad (38)$$

- Value-added tax, *VAT* (€/year), evaluated as the rate $v$ (%) applied to the sum of all the previous components.

The following case study implements the coefficients values presently in force (third quarter of 2017) and reported in Table 4. As a result, the correlation between the yearly purchased energy $E_A$ and the unit electricity price $c = C/E_A$ is reported in Figure 3. In the left graph, the plotted trends refer to a resident customer with increasing contractual power $P_{bill}$, whereas the cases of non-resident customers are reported in the right picture.

It is quite clear that the present Italian pricing structure for residential end-users weakly incentives the reduction of the yearly energy absorption only if $P_{bill}$ = 3 kW. In this case, the unit cost of electricity $c$ is lower in the range $E_1$–$E_2$ (1800–2640 kWh/year). For lower yearly purchases, the effect of fixed costs becomes dominant, whereas by increasing $E_A$ the policy on the energy components, depending on the introduced energy bracket (first of all, $C_{E,D}$ and $C_{S,E}$) and the rules for the excise duty computation, involve an increase in the electricity unit cost. Differently, in all the other cases (i.e., resident customers with $P_{bill}$ > 3 kW and non-resident customers), the unit cost of electricity decreases with high yearly absorptions due to the lower impact of both constant components and costs dependent on the customer contractual power $P_{bill}$. One of the advantages in reducing the end-user contractual power by suitably managing a BESS, i.e., discharging the batteries for supplying loads peaks when the local generation is not available, directly appears in the figure, since the unit price trend referred to $P_{bill}$ = 3 kW is significantly lower than the others.

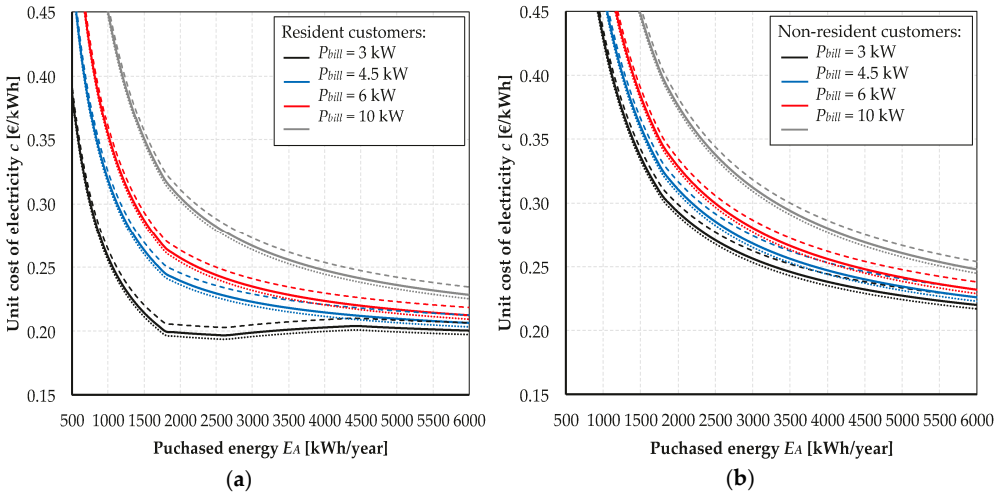


**Figure 3.** Correlation between the yearly absorption $E_A$ and the electricity unit cost $c = C/E_A$, with contractual power $P_{bill}$ equal to 3 kW, 4.5 kW, 6 kW, and 10 kW. (**a**) Resident customers; (**b**) Non-resident end-users. In both the figures, continuous lines represent the electricity unit cost adopting the ECP pricing method, whereas dotted lines and dashed lines refer to the TOU pricing mechanism (considering $E_{A1}/E_A$ = 0 and $E_{A1}/E_A$ = 1, respectively).

**Table 4.** Coefficients for the computation of the customer bill (values are defined by the Italian national authority and are updated to the third quarter of 2017).

| Bill Components | Coefficients | Resident Customers | | Non-Resident Customers | |
|---|---|---|---|---|---|
| Electricity consumption $C_E$ | $C_{E,0}$ (€/month) | 2.8869 | | 3.5788 | |
| | | TOU | ECP | TOU | ECP |
| | $c_{E,E1}$ (€/kWh) | 0.08441 | 0.07887 | 0.08441 | 0.07887 |
| | $c_{E,E2}$ (€/kWh) | 0.07607 | 0.07887 | 0.07607 | 0.07887 |
| | $c_{E,D1}$ up to $E_1$ (€/kWh) | 0.00272 | | 0 | |
| | $c_{E,D2}$ from $E_1$ to $E_2$ (€/kWh) | 0.00583 | | 0 | |
| | $c_{E,D3}$ from $E_2$ to $E_3$ (€/kWh) | 0.00583 | | 0 | |
| | $c_{E,D4}$ over $E_3$ (€/kWh) | 0.00583 | | 0 | |
| Electricity transportation and meter management $C_{TR}$ | $C_{TR,0}$ (€/month) | 1.58 | | 1.58 | |
| | $c_{TR,P}$ (€/kW month) | 1.8073 | | 1.8073 | |
| | $c_{TR,E1}$ up to $E_1$ (€/kWh) | 0.00842 | | 0.00842 | |
| | $c_{TR,E2}$ from $E_1$ to $E_2$ (€/kWh) | 0.00842 | | 0.00842 | |
| | $c_{TR,E3}$ from $E_2$ to $E_3$ (€/kWh) | 0.00842 | | 0.00842 | |
| | $c_{TR,E4}$ over $E_3$ (€/kWh) | 0.00842 | | 0.00842 | |
| Overall system costs coverage $C_S$ | $C_{S,0}$ (€/month) | 0 | | 10.6178 | |
| | $c_{S,E1}$ up to $E_1$ (€/kWh) | 0.025822 | | 0.025822 | |
| | $c_{s,E2}$ from $E_1$ to $E_2$ (€/kWh) | 0.057062 | | 0.057062 | |
| | $c_{s,E3}$ from $E_2$ to $E_3$ (€/kWh) | 0.057062 | | 0.057062 | |
| | $c_{s,E4}$ over $E_3$ (€/kWh) | 0.057062 | | 0.057062 | |
| Excise duty $C_{EX}$ | $c_{EX}$ (€/kWh) | 0.0227 | | 0.0227 | |
| $E_1$ = 1800 kWh/year, $E_2$ = 2640 kWh/year, $E_3$ = 4440 kWh/year<br>$E_{Ae1}$ = 1800 kWh/year, $E_{Ae2}$ = 2640 kWh/year, $v$ = 10% | | | | | |

### *4.2. Sold Energy Remuneration*

Considering that net-metering advantages are expected to be extinguished in the near future, the algorithm assigns the unit value $r_I$ (€/kWh) to the energy injected into the main grid $E_I$. Therefore, the revenue obtained by selling the generation surplus $R_I$ (€/year) is computed by Equation (39).

$$R_I = r_I \, E_I \tag{39}$$

## 5. Case Study and Results

### *5.1. End-User Characteristics*

The behavior of a real passive end-user on a yearly time period has been used (base case, Scenario A). The active power profile is obtained by collecting the power absorption at the PoD with a time resolution of a quarter-of-an-hour, i.e., $\Delta t$ = 0.25 h. In Figure 4, three weekly profiles referring to winter (third full week of December), spring (third full week of March), and summer (third full week of June) are reported. The figure depicts the load consumption with a negative sign ($-P_L$(t)) to obtain a clearer representation.

Considering the entire year, the load power absorption varies in the range 0/3.64 kW. Consequently, the contractual power $P_{bill}$ is set to 4.5 kW in the passive configuration. The yearly consumption $E_A$ is 4448 kWh/year ($E_{A1}$ = 1303 kWh/year and $E_{A2}$ = 3145 kWh/year). Without local generation and storage, the yearly customer bill $C$ is equal to 944.22 €/year, adopting the ECP Italian pricing mechanism (942.48 €/year according to the regulated Italian TOU approach). Since no significant variations between the ECP approach and the TOU pricing mechanism are appreciable as a consequence of the values assigned by the Italian energy authority, the following results refer to the ECP bill computation.

### 5.2. PV Plant Characteristics and Main Outputs

A real PV plant with rated power $P_{PV,r}$ equal to 4.0 kW and panels surface with tilt angle 15° and azimuth angle 10° (southwest orientation) is considered. The plant is located in Northern Italy as the passive customer, and thus the influences of the local weather on both the load profile and the solar availability are considered equally. In Figure 4, the seasonal variations of the PV production trends are appreciable with reference to three characteristic weeks.

The yearly solar radiation measured on the PV panel surface is 1564 kWh/(m$^2$ year) and the PV cell temperature profile is available ($T_C$ in the range −5.7/66.4 °C depending on daily and seasonal variations). PV panels make use of Si-poly cells (PV conversion efficiency 16.8%) and $\gamma$ = −0.45%/°C. In the case that only the PV plant is installed by the passive customer (Scenario B), the PV production on the DC side of the DC/AC inverter is 5299 kWh/year since $\eta_{BOS}$ = 92% is considered. The inverter-rated power $S_{I,r}$ is equal to 4.0 kVA according to the PV characteristics. The DC/AC efficiency curve depending on its loading rate is considered, thus resulting in an AC production equal to 5167 kWh/year, i.e., the PV unitary production is 1292 kWh/(kW year).

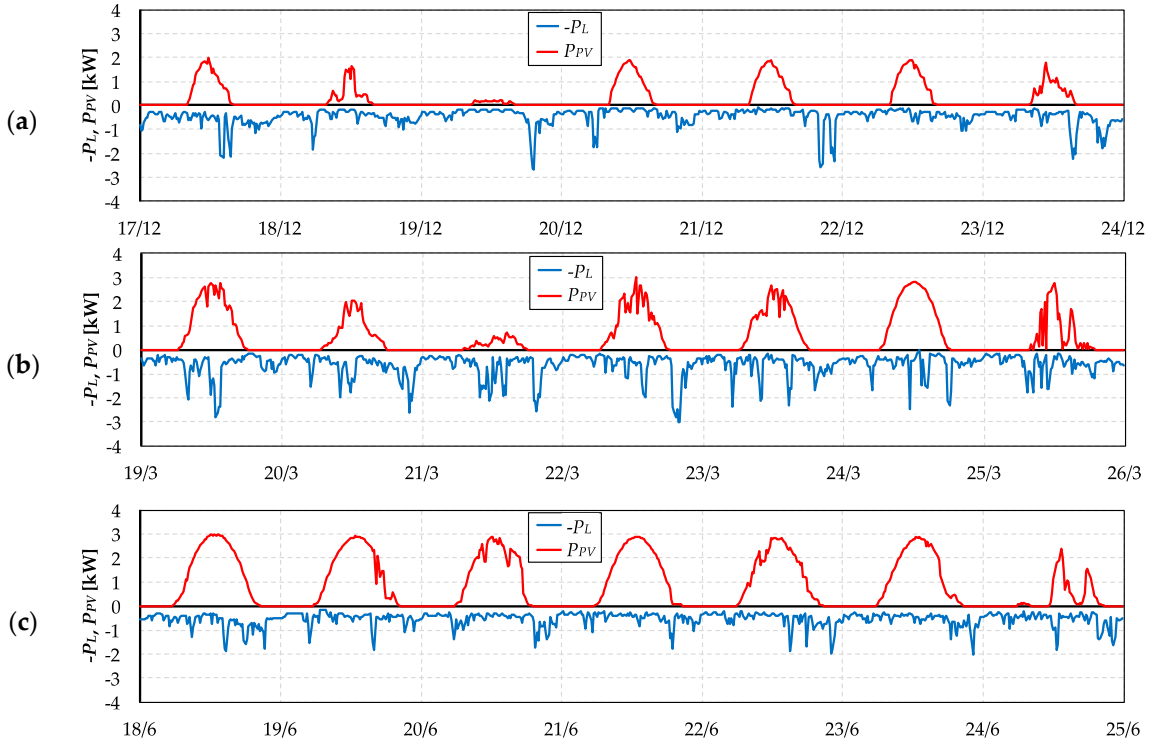


**Figure 4.** Representation of the weekly profiles of the load power consumption $-P_L(t)$ (blue lines) and the PV production ($P_{PV}(t) = P_{I,AC}(t)$ without BESS, red lines), for three typical seasons: (**a**) the third full week of December; (**b**) the third full week of March; and (**c**) the third full week of June. Sundays are reported as the last days of the depicted time windows.

Only a minor part of the PV production (1468 kWh/year, 28.4% of the PV production, and 33.0% of the load consumption) is immediately self-consumed by the customer loads due to the opposite power trends of the load consumption and the PV generation. However, the installation of the sole PV unit allows the end-user to reduce its yearly energy absorption from the distribution network $E_A$ to 2977 kWh/year. Since the PV generation is concentrated in the central hours of the day, whereas the load peaks are in the evening, the contractual power $P_{bill}$ cannot be reduced by the installation of the sole PV unit. The annual bill for purchased electricity drops down to 664.41 €/year, whereas a revenue of 147.94 €/year due to the injection of the PV surplus into the network ($E_I$ = 3699 kWh/year)

is obtained (unit selling price $r_I$ = 0.04 €/kWh). Thus, the PV installation makes available an overall economic benefit of 427.75 €/year.

### 5.3. BESS Characteristics and Obtained Benefits

The storage unit based on the $NaNiCl_2$ technology (battery model VAC160, FZSONICK SA, Stabio, Switzerland) considers the rated characteristics reported in Table 5. The modeled thermal behaviors during discharging phases, reported in Figure 2b, completely represent the field measurements depicted in Figure 2a. The DC/DC converter has rated power $S_{DC,r}$ equal to 3 kW, and its efficiency curve is modeled similarly to the DC/AC converter. The admitted SoC range allows for the preservation of the BESS lifetime in terms of the admitted number of complete charging/discharging cycles, typically set at 4500 cycles for the $NaNiCl_2$ technology. The charging and discharging efficiencies ($\eta_C$ and $\eta_D$, respectively) are compliant with the rated charging/discharging roundtrip efficiency of the selected battery model (88%).

**Table 5.** Rated characteristics of the $NaNiCl_2$-based BESS considered in the case study.

| Parameter (Unit of Measure) | Value |
|---|---|
| Storable energy in rated conditions, $E_B$ (kWh) | 7.6 |
| Minimum admitted internal temperature, $T_m$ (°C) | 265 |
| Maximum admitted internal temperature, $T_M$ (°C) | 320 |
| Initial internal temperature, $T_B(0)$ (°C) | 265 |
| Battery hourly cooling rate $T_S$, at $T_B$ = 300 °C (°C/h) | 4 |
| Minimum admitted State of Charge, $SoC_m$ (%) | 10% |
| Maximum admitted State of Charge, $SoC_M$ (%) | 90% |
| Initial State of Charge, $SoC(0)$ (%) | 50% |
| Battery efficiency during the discharging phase, $\eta_D$ (%) | 90% |
| Battery efficiency during the charging phase, $\eta_C$ (%) | 98% |
| Rated discharging power, $P_{D,r}$ (kW) | 3.35 |
| Rated charging power, $P_{C,r}$ (kW) | 1.89 |
| Battery heater rated power, $P_{H,r}$, at $T_B$ = 300 °C (kW) | 0.05 |

Considering the integrated management of the PV-BESS system (Scenario C), Figure 5 reports an example of the storage system management strategy, referring to two consecutive spring days with different trends of sunny radiation (24 and 25 March). The BESS controller operates locally, based only on customer measurements since no information, requirements, or market signals are supposed to be exchanged with the external environment, e.g., with the DSO for supplying ancillary services. Consequently, the storage unit is charged ($P_B < 0$, bold black time trend in Figure 5b) with the PV surplus (when the red line overpasses the blue line in Figure 5a) until the maximum admitted SoC threshold $SoC_M$ is reached (Figure 5c) and according to the admitted charging rate $P_{Cmax}$ evaluated as in Equation (12) and graphically reported in Figure 5b (dotted line). Similarly, the BESS discharges during the evening and the night to supply the load up to the minimum SoC value $SoC_m$ and taking into account the maximum discharging rate $P_{Dmax}$ (dashed line in Figure 5b) evaluated in Equation (11). In the case of charge, stand-by, or very weak discharge, the internal temperature $T_B$ (Figure 5d) decreases according to Equation (10) and the battery heater is switched on to avoid over-cooling (Figure 5e) if $T_B$ is close to $T_m$. In Figure 5f, the profile of the power exchanged with the public network $P_{PoD}$ is reported in the cases the BESS is operative (Scenario C, bold black line) or not (Scenario B, dotted grey line).

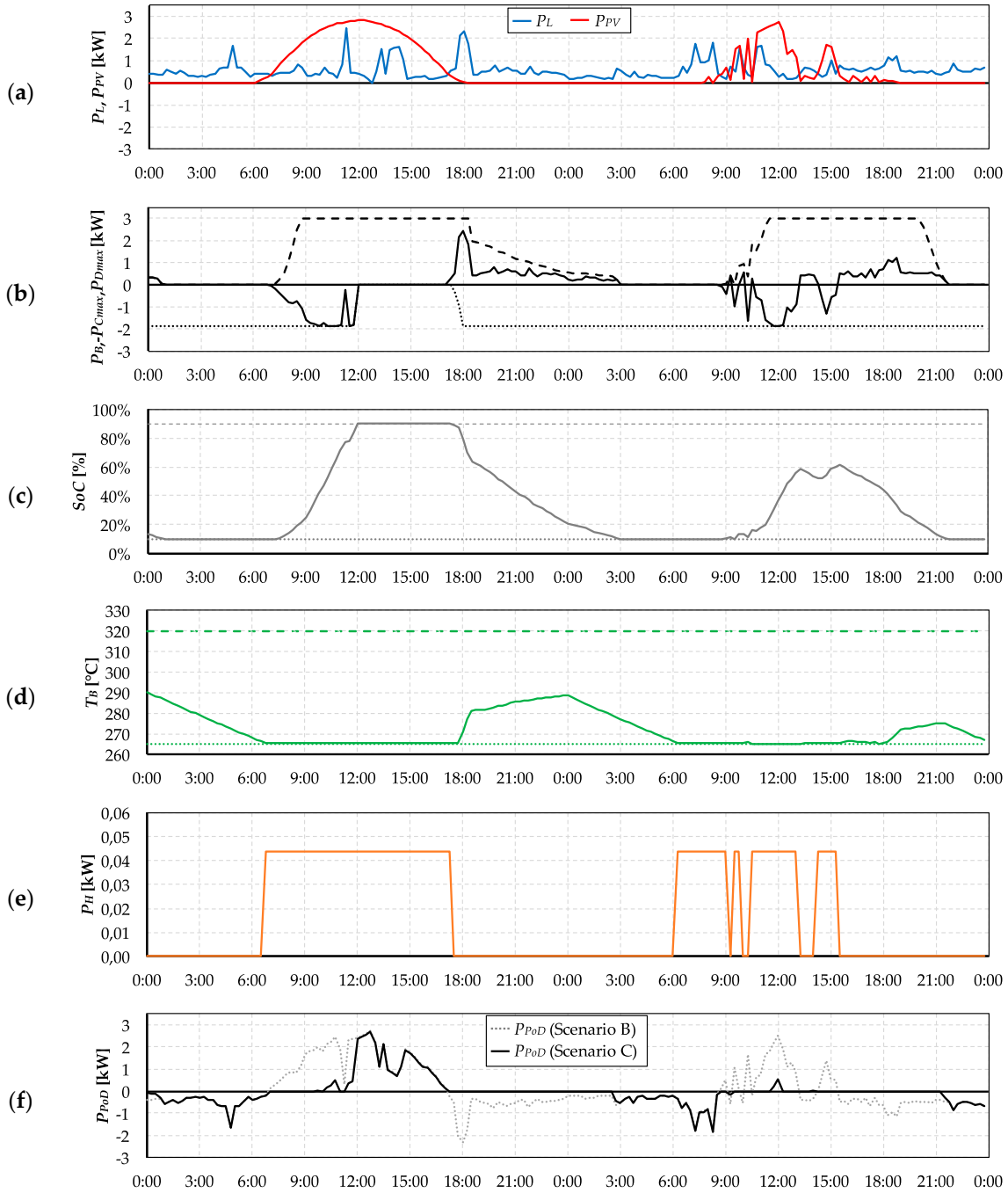


**Figure 5.** Graphical representation of the BESS operation during a couple of spring days (24 and 25 March). (**a**) PV generation (red line) and load consumption $P_L(t)$ (blue line); (**b**) Battery power flow $P_B(t)$ (bold black line), dynamic charging constraint $-P_{Cmax}(t)$ (dotted black line) and dynamic discharging constraint $P_{Dmax}(t)$ (dashed black line); (**c**) State of Charge time trend $SoC(t)$ (bold grey line) and its admitted range defined by $SoC_m$ and $SoC_M$ (dotted line and dashed line, respectively); (**d**) Internal temperature behavior $T_B(t)$ (bold green line) and its admitted range defined by $T_m$ and $T_M$ (dotted line and dashed line, respectively); (**e**) Battery heater power absorption $P_H(t)$; (**f**) Power exchange time trend $P_{PoD}(t)$ in cases where the BESS is operative (bold black line) or not (dotted grey line).

Operating the BESS with these rules, the power exchanges with the public network are dramatically reduced. In Figure 6, the statistical distributions of the power $P_{PoD}$ are represented

in the form of bar graphs referring to the three studied scenarios. It is clearly confirmed that the installation of the sole PV unit (yellow bar diagrams) decreases the amount of purchased energy in comparison with the passive customer (grey bar diagrams), even though the absorption peaks are not reduced. At the same time, the PV generation causes the active power injection into the grid in a significant amount of time, in particular during the spring-summer period (upper image of Figure 6b). The BESS plays a fundamental role in reducing the power exchanges between the end-user and the public network, in terms of both power absorption and power injection. It worth noting that $P_{PoD}$ remains in the power band $-0.125/0.125$ kW for about 50.8% of the overall time (4452 h/year) in Scenario C.

In addition, since the storage unit is able to supply the evening load requirements, the maximum absorbed power is reduced and consequently the customer is able to lower the contractual power $P_{bill}$ to 3 kW. This means that a benefit in terms of electricity unit cost is directly obtained, since, referring to Figure 3, the customer bill is now evaluated on the black line instead of on the blue trend (as required in Scenarios A and B).

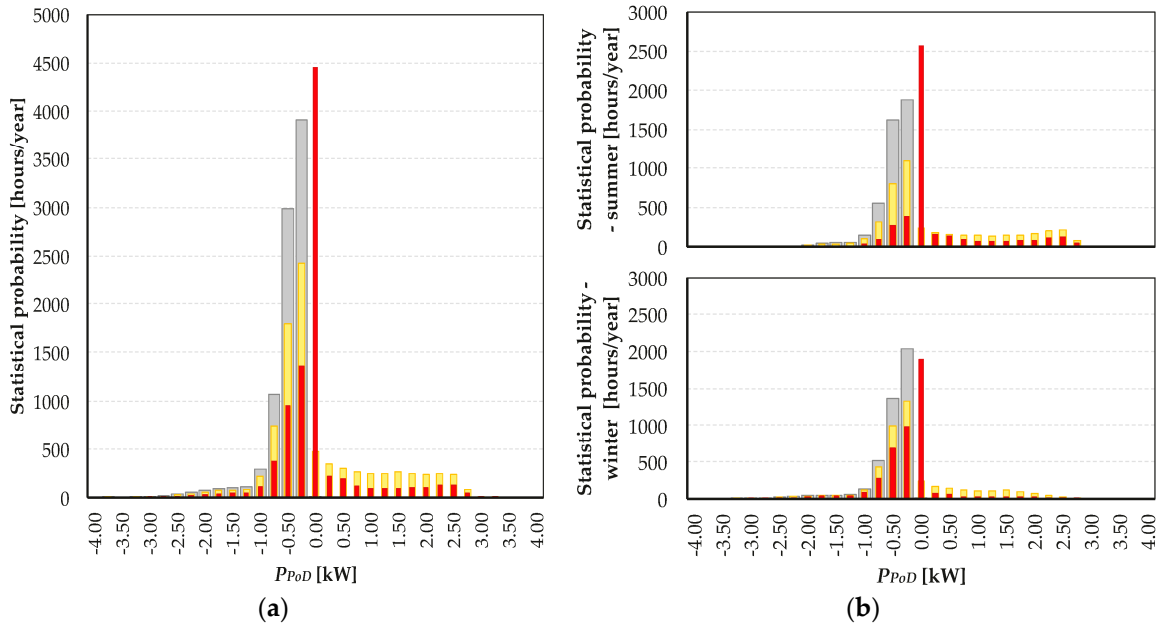


**Figure 6.** Statistical distribution of the power flow $P_{PoD}$ exchanged between the final customer and the network, for the three analyzed scenarios ($P_{PoD} > 0$ means power injection into the grid). With a BESS, $P_{PoD}$ is frequently close to zero, thus limiting the end-user impact on network management issues, (e.g., voltage regulation and distribution losses). (**a**) Yearly statistical distribution; (**b**) Spring-summer statistical distribution (upper image), and fall-winter statistical distribution (lower image).

The effectiveness of the BESS in containing the energy exchanges is confirmed in Figure 7, in which the daily amounts of absorbed energy (blue bars, reported as negative to assure the clarity of the image) and injected energy (green bars) are depicted. Taking into account the peculiarities of real power trends, both in terms of consumption (week variations, holidays, etc.) and production (seasonal variations, real weather conditions, etc.), it clearly appears that the storage unit dramatically reduces the customer absorption during the summer (when the SoC is frequently kept high due to the significant availability of solar energy, thus, the end-user rarely absorbs energy from the public network). Oppositely, during the winter period, the PV overproduction is almost never injected into the grid. In other words, from the DSO's perspective, the active customer equipped with a BESS is equivalently representable as a pure PV generator during the central section of the year (with equivalent rated power lower than $P_{PV,r}$) and as a passive end-user during the fall-winter period (with limited energy absorption in comparison with Scenario A).

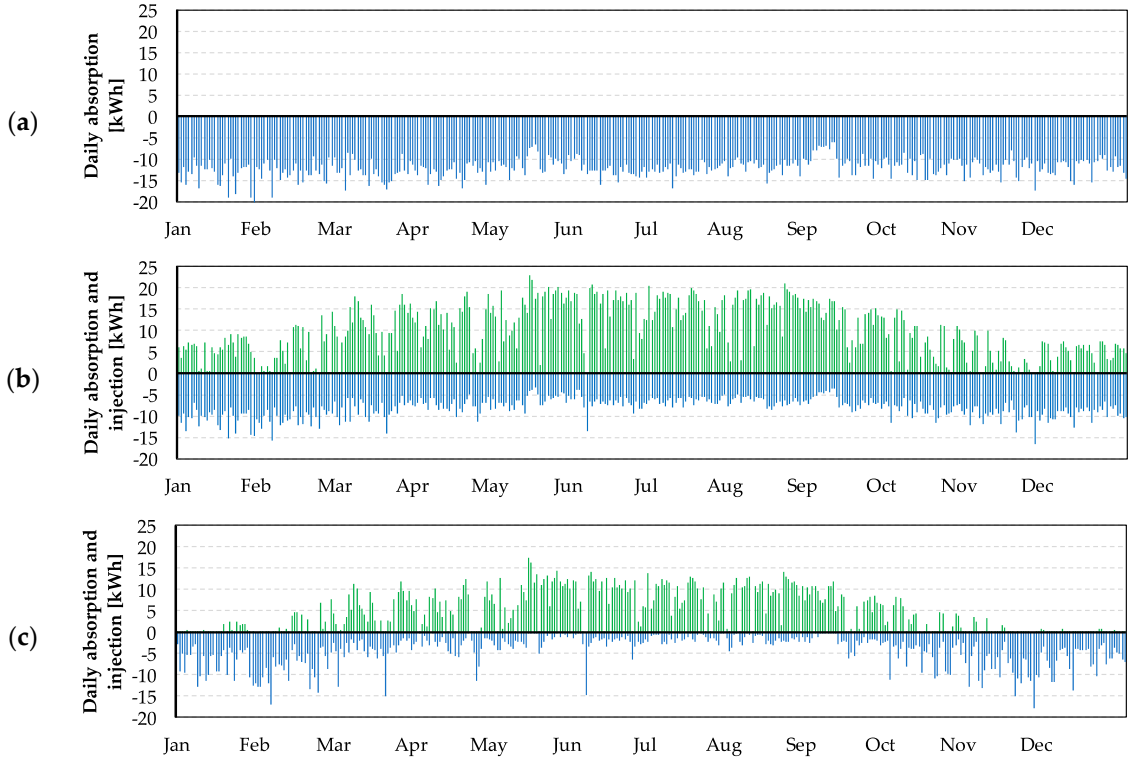


**Figure 7.** Daily energy absorption (blue bars, reported as negative terms for the aim of clarity) and daily energy injection (green bars). (**a**) Scenario A, passive end-user; (**b**) Scenario B, customer with the sole PV generation; (**c**) Scenario C, active end-user equipped with PV generation and storage.

Moreover, one of the benefits of a BESS, when it is managed to maximize the self-consumption of the PV generation, is the reduction of the variability of the power exchange with the public network, i.e., the overall end-user is more programmable and causes limited perturbation in the network operating conditions. In the presented case study, the parameter $\Delta P_{PoD}$ is equal to 0.163 kW in the passive configuration, increases to 0.212 kW in the presence of the sole PV unit (Scenario B), and decreases to 0.124 kW in the Scenario C. This means that the results of the end-user equipped with the BESS are significantly less variable than those in the passive configuration.

On a yearly basis, the $NaNiCl_2$-based BESS increases the amount of self-supplied energy to 2870 kWh/year (64.5% of the overall load consumption), limits the PV surplus injected into the public network to 1713 kWh/year, and reduces the purchased energy to 1578 kWh/year. These final values include both the charging/discharging efficiencies of the storage system and its thermal consumption to preserve the internal temperature $T_B$ from dangerous cooling ($E_H$ = 229.7 kWh/year). It is important to note that the thermal regulation of the battery internal temperature has a very limited impact in economic terms (17.73 €/year) since about half of $E_H$ (106.7 kWh/year) is required during diurnal hours (when the battery is charged and later kept in stand-by conditions after the maximum SoC has been reached, as shown in the first day depicted in Figure 5e). This means that a significant part of the thermal regulation is realized by making use of the PV surplus (weakly evaluated on the market once net-metering incentivizing policies will be retired).

The annual bill passes from 944.22 €/year to 331.63 €/year and the income from selling the PV surplus is 68.52 €/year, which means that the PV + BESS configuration has an overall benefit of 681.10 €/year in comparison with the passive configuration (+253.35 €/year compared to Scenario B).

The management strategy does not compromise the storage system lifetime, since the yearly aging of the battery $A$ is limited to 213.5 equivalent cycles, taking into account that partial cycles are required in the case of either reduced daily load consumption or low solar availability (as in the second day depicted in Figure 5). Furthermore, no overheating issues are recorded during the yearly operation

of the BESS and the upper threshold $T_M$, added in the management procedure as a precaution, is never reached since the customer loads rarely require very large amounts of power for several hours, as confirmed by the statistical distribution of the internal temperature $T_B$ reported in Figure 8.

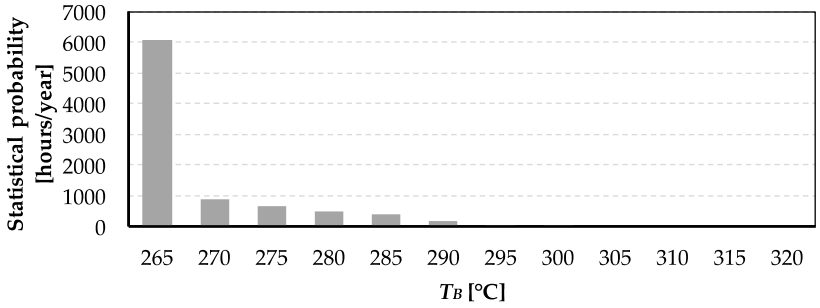


**Figure 8.** Statistical distribution of the battery internal temperature $T_B$, in comparison with the admitted range $T_m/T_M$.

The SoC statistical distribution is reported in the form of a bar diagram in Figure 9. From the individual analysis of the spring-summer season (yellow bars in Figure 9b) and the fall-winter period (light blue bars in Figure 9b), realizing the BESS through a couple of batteries operating in parallel could be an interesting alternative to significantly reduce the overall heating consumption. With this storage system architecture, one of the batteries could be switched off in the months in which the BESS rarely reaches the highest threshold $SoC_M$ due to the low solar availability.

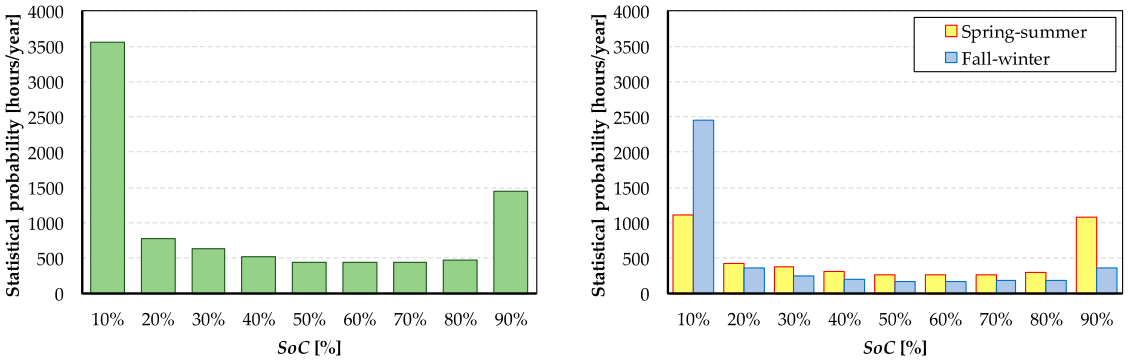


**Figure 9.** State of charge. (**a**) Yearly statistical distribution; (**b**) Statistical distributions considering the spring-summer period and the fall-winter period.

Additionally, the impact of seasonal variations of both the PV availability and load demand is summarized in Table 6, which reports the monthly trends of representing parameters *SSR*, *SCR*, and *MSF*. Even if this paper refers to different environmental conditions and it adopts a more accurate battery thermal model, its results have significant similarities with Reference [48].

For the purpose of easily comparing the considered scenarios and better appreciating the impact of the $NaNiCl_2$ BESS on end-user management and costs, Table 7 summarizes all of the obtained results in terms of technical and economic aspects.

**Table 6.** Monthly trend of representing parameters *SSR*, *SCR*, and *MSF* in Scenario B and in Scenario C (all of these parameters are dimensionless), related to monthly data of load consumption and PV energy injected in the DC bus.

| Month | Load Consumption (kWh) | PV DC Production (kWh) | Scenario B (PV plant) | | Scenario C (PV Plant + BESS) | | |
|---|---|---|---|---|---|---|---|
| | $\sum P_L(t)\Delta t$ | $\sum P_{PV}(t)\Delta t$ | *SSR* | *SCR* | *SSR* | *SCR* | *MSF* |
| January | 424 | 269 | 21.8% | 36.7% | 47.7% | 94.4% | 55.5% |
| February | 367 | 209 | 20.3% | 38.3% | 35.6% | 84.7% | 67.1% |
| March | 403 | 492 | 33.3% | 29.6% | 67.1% | 68.1% | 39.7% |
| April | 392 | 517 | 42.3% | 34.5% | 76.1% | 70.1% | 31.4% |
| May | 341 | 624 | 41.5% | 25.2% | 82.4% | 55.9% | 23.0% |
| June | 380 | 627 | 44.5% | 29.4% | 81.2% | 59.4% | 27.3% |
| July | 387 | 675 | 48.1% | 30.0% | 88.8% | 61.1% | 21.7% |
| August | 360 | 662 | 43.1% | 25.8% | 84.6% | 56.3% | 25.0% |
| September | 302 | 499 | 36.0% | 24.2% | 81.0% | 62.0% | 23.8% |
| October | 367 | 323 | 27.5% | 33.8% | 55.0% | 79.5% | 51.2% |
| November | 360 | 170 | 18.4% | 41.8% | 30.3% | 92.2% | 71.7% |
| December | 366 | 232 | 21.1% | 35.6% | 47.9% | 98.3% | 56.9% |
| Overall year | 4448 | 5299 | 33.1% | 30.2% | 64.5% | 67.7% | 41.0% |

**Table 7.** Main results obtained by adopting the developed simplified thermoelectric model of the sodium-nickel chloride BESS to a real case residential prosumer, in the considered scenarios (annual analysis).

| Parameter (Unit of Measure) | Scenario A (Passive End-User) | Scenario B (PV Plant) | Scenario C (PV Plant + BESS) |
|---|---|---|---|
| PV plant rated power, $P_{PV,r}$ (kW) | – | 4.0 | 4.0 |
| Storable energy in rated conditions, $E_B$ (kWh) | – | – | 7.6 |
| Load consumption, $E_L$ (kWh) | 4448 | 4448 | 4448 |
| Absorbed energy in peak hours, $E_{A1}$ (kWh) | 1303 | 361 | 165 |
| Absorbed energy in off-peak hours, $E_{A2}$ (kWh) | 3145 | 2616 | 1414 |
| Overall absorbed energy at the PoD, $E_A$ (kWh) | 4448 | 2977 | 1578 |
| Maximum power absorption (kW) | 3.64 | 3.64 | 2.79 |
| End-user contractual power, $P_{bill}$ (kW) | 4.5 | 4.5 | 3.0 |
| PV energy injected in the DC bus, $E_{PV}$ (kWh) | – | 5296 | 5296 |
| Self-sufficiency ratio *SSR* (dimensionless) | 0.0% | 33.1% | 64.5% |
| Self-consumed PV production (kWh) | – | 1468 | 2870 |
| Injected energy at the PoD (kWh) | – | 3698 | 1713 |
| Self-consumption ratio, *SCR* (dimensionless) | – | 30.2% | 67.7% |
| Heater energy consumption, $E_H$ (kWh) | – | – | 230 |
| Economic impact of heater energy consumption (€/year) | – | – | 17.73 |
| Battery aging, A (cycles) | – | – | 213.5 |
| Average variation of power exchange at the PoD between subsequent time instants, $\Delta P_{PoD}$ (kW) | 0.163 | 0.212 | 0.124 |
| Customer bill, component, $C_E$ (€/year) | 405.81 | 281.18 | 163.41 |
| Customer bill, component, $C_{TR}$ (€/year) | 154.00 | 141.62 | 97.31 |
| Customer bill, component, $C_S$ (€/year) | 197.59 | 113.63 | 40.75 |
| Customer bill, component, $C_{EX}$ (€/year) | 100.97 | 67.57 | 0.00 |
| Customer bill, *VAT* (€/year) | 85.84 | 60.40 | 30.15 |
| Overall customer bill, *C* (€/year) | 944.22 | 664.41 | 331.63 |
| Revenue of injected energy, $R_I$ (€/year) | – | 147.94 | 68.52 |
| Economic benefit in comparison with Scenario A | – | 427.75 | 681.10 |
| Economic benefit in comparison with Scenario B | – | – | 253.35 |

Finally, the three scenarios are depicted in Figure 10 in terms of annual bill. For each scenario, the bill main components $C_E$, $C_{TR}$, $C_S$, $C_{EX}$, and *VAT* are reported in clockwise order in the five-axes representation, where $C_E$ is located on the vertical axis. For each component, the fixed amount is represented with the red line. Referring to a residential supplying contract, in Figure 10, a red triangle is graphically obtained in each scenario because only $C_E$ and $C_{TR}$ have fixed sub-components, i.e., $C_{E,0}$

and $C_{TR,0}$, respectively. Since the red polygon represents fixed costs, it is not alterable by installing either the PV generator or the BESS. Blue polygons represent the sum of fixed components and power components, which means that the amount ($12 \cdot C_{TR,P}$) is added to the red polygons along the axis $C_{TR}$. Since the BESS allows for a reduction of the contractual power $P_{bill}$ in Scenario C, this economic advantage is represented in Figure 10c, where the blue triangle is smaller as regards to Figure 10a,b.

For each scenario, the black pentagon crosses the five axes at the correspondent bill main components $C_E$, $C_{TR}$, $C_S$, $C_{EX}$ and $VAT$. The progressive reduction in the yearly energy absorption $E_A$ moving from Scenario A to Scenario C directly reduces the size of the black polygon. When several energy brackets are applied on the computation of specific energy-dependent components (e.g., $C_{S,E}$ and $C_{E,D}$, which is a part of $C_{E,E}$), their reductions with the decrease of $E_A$ are more than proportional. Moreover, the formulation of $C_{EX}$ allows the end-user to be excused from the payment of the excise duty in Scenario C, since the BESS operation reduces the customer annual absorption under the complete exemption threshold for resident customers (as appreciable in Figure 10c).

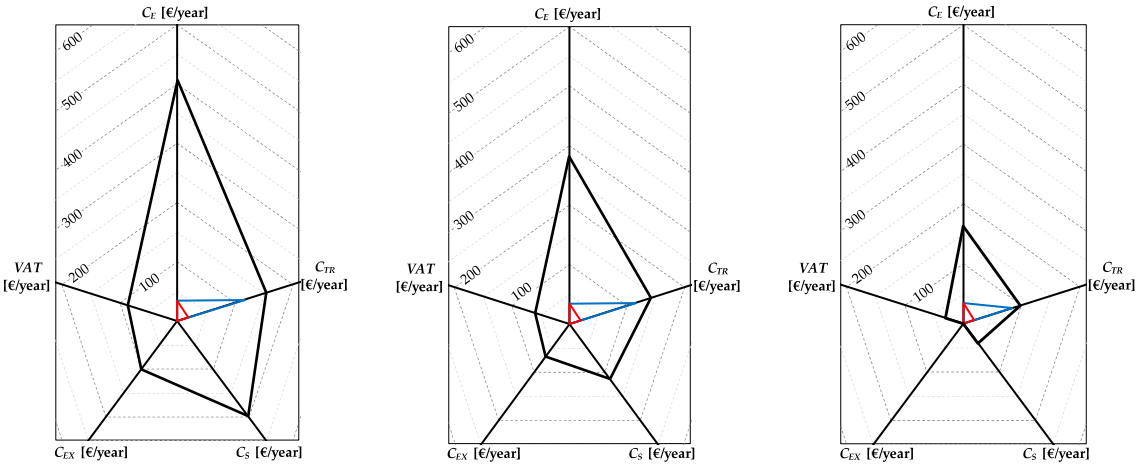


**Figure 10.** Bill components $C_E$, $C_{TR}$, $C_S$, $C_{EX}$, and $VAT$ represented in a five-axes plan. (**a**) Scenario A, passive customer; (**b**) Scenario B, active end-user solely with PV generation; (**c**) Scenario C, active end-users with PV generation and storage system.

## 6. Conclusions

The paper thoroughly describes a model able to contemporarily characterize both the power flow management of a sodium-nickel chloride battery (here installed to optimize the prosumer self-consumption) and its thermal behavior. The procedure suitably takes into account the mutual relation between these two aspects, since the internal temperature limits the discharging power, whereas the amount of power exchanged at the battery terminals influences the internal temperature.

The developed model and the proposed procedure applied to real quarter-hour power profiles of both customer consumption and PV availability confirm the interest in applying the sodium-nickel chloride technology at the household level. Referring to the Italian context, the study demonstrates that a significant increase of the self-consumption rate is obtained, giving rise to an annual economic income which partially covers both installation and maintenance costs of the storage unit. In comparison with other storage technologies, the sodium-nickel chloride battery constraints in terms of the internal temperature admitted range do not compromise the annual revenue of the investment in a detrimental way, since the yearly cost for adjusting the battery internal temperature is limited to a few percentage points of the annual bill. In addition, by adopting a BESS, the active customer bill becomes more independent of possible variations in the electricity market price, whereas locally-introduced incentivizing policies could have a role in equivalently lowering the installation cost. These considerations could make the installation of a BESS attractive from the customer's point of

view, in combination with the ability of BESSes to provide back-up supply and the participation in the future ancillary services market. However, a specific business case needs to be performed according to both the end-user main characteristics (e.g., annual purchase of electricity, customer load profiles, PV production profiles, etc.) and the locally-applied policies, in terms of: (i) admitted power exchanges between the end-user and the distribution network; (ii) purchasing and selling price mechanisms; (iii) incentivizing policies; and (iv) connection rules.

**Author Contributions:** Fabio Bignucolo and Giorgio Crugnola conceived the study. Fabio Bignucolo, Massimiliano Coppo, and Andrea Savio developed the equivalent thermoelectric model of the sodium-nickel chloride battery applied to residential customers, working in the MATLAB® environment. Giorgio Crugnola supported the research activity making available real measurements of laboratory tests on the considered battery model. All the authors wrote, reviewed, and approved the manuscript.

**Conflicts of Interest:** The founding sponsor had no role in the design of the study; in the collection, analyses, or interpretation of data; in the writing of the manuscript, and in the decision to publish the results.

## References

1. International Energy Agency (IEA). *World Energy Outlook 2013*; OECD/IEA: Paris, France, 2013.
2. Moura, P.S.; López, G.L.; Moreno, J.I.; De Almeida, A.T. The role of smart grids to foster energy efficiency. *Energy Effic.* **2013**, *6*, 621–639. [CrossRef]
3. Lang, T.; Ammann, D.; Girod, B. Profitability in absence of subsidies: A techno-economic analysis of rooftop photovoltaic self-consumption in residential and commercial buildings. *Renew. Energy* **2016**, *87*, 77–87. [CrossRef]
4. Riesen, Y.; Ballif, C.; Wyrsch, N. Control algorithm for a residential photovoltaic system with storage. *Appl. Energy* **2017**, *202*, 78–87. [CrossRef]
5. Olaszi, B.D.; Ladanyi, J. Comparison of different discharge strategies of grid-connected residential PV systems with energy storage in perspective of optimal battery energy storage system sizing. *Renew. Sustain. Energy Rev.* **2017**, *75*, 710–718. [CrossRef]
6. Vieira, F.M.; Moura, P.S.; de Almeida, A.T. Energy storage system for self-consumption of photovoltaic energy in residential zero energy buildings. *Renew. Energy* **2017**, *103*, 308–320. [CrossRef]
7. Castillo-Cagigal, M.; Caamaño-Martín, E.; Matallanas, E.; Masa-Bote, D.; Gutiérrez, A.; Monasterio-Huelin, F.; Jiménez-Leube, J. PV self-consumption optimization with storage and Active DSM for the residential sector. *Solar Energy* **2011**, *85*, 2338–2348. [CrossRef]
8. Bignucolo, F.; Savio, A.; Turri, R.; Pesavento, N.; Coppo, M. Influence of Electricity Pricing Models on the Daily Optimization of Residential End-Users integrating Storage Systems. In Proceedings of the 7th International Conference on Modern Power Systems 2017, Cluj-Napoca, Romania, 6–9 June 2017.
9. Bignucolo, F.; Caldon, R.; Sacco, A. A novel market based Distribution System controller for active distribution networks. In Proceedings of the 44th International Universities Power Engineering Conference (UPEC), Glasgow, UK, 1–4 September 2009.
10. Barbato, A.; Capone, A. Optimization Models and Methods for Demand-Side Management of Residential Users: A Survey. *Energies* **2014**, *7*, 5787–5824. [CrossRef]
11. Esther, B.P.; Kumar, K.S. A survey on residential Demand Side Management architecture, approaches, optimization models and methods. *Renew. Sustain. Energy Rev.* **2016**, *59*, 342–351. [CrossRef]
12. Ahmad, A.; Khan, A.; Javaid, N.; Hussain, H.M.; Abdul, W.; Almogren, A.; Alamri, A.; Azim Niaz, I. An Optimized Home Energy Management System with Integrated Renewable Energy and Storage Resources. *Energies* **2017**, *10*, 549. [CrossRef]
13. Sheikhi, A.; Rayati, M.; Ranjbar, A.M. Demand side management for a residential customer in multi-energy systems. *Sustain. Cities Soc.* **2016**, *22*, 63–77. [CrossRef]
14. Damiano, A.; Gatto, G.; Marongiu, I.; Porru, M.; Serpi, A. Real-Time Control Strategy of Energy Storage Systems for Renewable Energy Sources Exploitation. *IEEE Trans. Sustain. Energy* **2014**, *5*, 567–576. [CrossRef]
15. Shen, J.; Jiang, C.; Li, B. Controllable Load Management Approaches in Smart Grids. *Energies* **2015**, *8*, 11187–11202. [CrossRef]
16. Ogunjuyigbe, A.S.O.; Ayodele, T.R.; Akinola, O.A. User satisfaction-induced demand side load management in residential buildings with user budget constraint. *Appl. Energy* **2017**, *187*, 352–366. [CrossRef]

17. Yang, F.; Xia, X. Techno-economic and environmental optimization of a household photovoltaic-battery hybrid power system within demand side management. *Renew. Energy* **2017**, *108*, 132–143. [CrossRef]
18. Bignucolo, F.; Caldon, R.; Carradore, L.; Sacco, A.; Turri, R. Role of storage systems and market based ancillary services in active distribution networks management. In Proceedings of the 43rd International Conference on Large High Voltage Electric Systems (CIGRE), Paris, France, 22–27 August 2010.
19. Caldon, R.; Coppo, M.; Turri, R. Voltage unbalance compensation in LV networks with inverter interfaced distributed energy resources. In Proceedings of the 2012 IEEE International Energy Conference and Exhibition (ENERGYCON), Florence, Italy, 9–12 September 2012; pp. 527–532.
20. Bignucolo, F.; Savio, A.; Caldon, R. Contribution of MV Static Distributed Generation to Voltage Unbalance Mitigation. In Proceedings of the 2016 AEIT International Annual Conference (AEIT), Naples, Italy, 5–7 October 2016.
21. Behera, M.P.; Ray, P.K.; Beng, G.H. Three-phase shunt connected Photovoltaic generator for harmonic and reactive power compensation with battery energy storage device. In Proceedings of the IECON 2016—42nd Annual Conference of the IEEE Industrial Electronics Society, Florence, Italy, 23–26 October 2016; pp. 2408–2413.
22. Milanes-Montero, M.-I.; Barrero-Gonzalez, F.; Pando-Acedo, J.; Gonzalez-Romera, E.; Romero-Cadaval, E.; Moreno-Munoz, A. Active, Reactive and Harmonic Control for Distributed Energy Micro-Storage Systems in Smart Communities Homes. *Energies* **2017**, *10*, 448. [CrossRef]
23. Lammert, G.; Heß, T.; Schmidt, M.; Schegner, P.; Braun, M. Dynamic grid support in low voltage grids-fault ride-through and reactive power/voltage support during grid disturbances. In Proceedings of the Power Systems Computation Conference (PSCC), Wroclaw, Poland, 18–22 August 2014.
24. Kermani, M. Transient voltage and frequency stability of an isolated microgrid based on energy storage systems. In Proceedings of the 2016 IEEE 16th International Conference on Environment and Electrical Engineering (EEEIC), Florence, Italy, 7–10 June 2016.
25. Bignucolo, F.; Raciti, A.; Caldon, R. Coordinating active and reactive energy balances in islanded networks supported by renewables and BESS. In Proceedings of the 3rd IET Renewable Power Generation Conference, Naples, Italy, 24–25 September 2014.
26. European Committee for Electrotechnical Standardization. Technical Specification CENELEC TS 50549–1. In *Requirements for Generating Plants to Be Connected in Parallel with Distribution Networks—Part 1: Connection to a LV Distribution Network above 16 A*; CENELEC: Brussels, Belgium, 2015.
27. Comitato Elettrotecnico Italiano, CEI 0–21. *Reference Technical Rules for the Connection of Active and Passive Users to the LV Electrical Utilities*; CEI: Milan, Italy, 2016.
28. Bignucolo, F.; Cerretti, A.; Coppo, M.; Savio, A.; Turri, R. Impact of Distributed Generation Grid Code Requirements on Islanding Detection in LV Networks. *Energies* **2017**, *10*, 156. [CrossRef]
29. Bignucolo, F.; Cerretti, A.; Coppo, M.; Savio, A.; Turri, R. Effects of Energy Storage Systems Grid Code Requirements on Interface Protection Performances in Low Voltage Networks. *Energies* **2017**, *10*, 387. [CrossRef]
30. European Committee for Electrotechnical Standardization, Technical Specification CENELEC TS 50549-2. *Requirements for Generating Plants to Be Connected in Parallel with Distribution Networks–Part 2: Connection to a MV Distribution System*; CENELEC: Brussels, Belgium, 2015.
31. Comitato Elettrotecnico Italiano, CEI 0–16. *Reference Technical Rules for the Connection of Active and Passive Consumers to the HV and MV Electrical Networks of Distribution Company*; CEI: Milan, Italy, 2016.
32. Dufo-López, R.; Bernal-Agustín, J.L. Techno-economic analysis of grid-connected battery storage. *Energy Convers. Manag.* **2015**, *91*, 394–404. [CrossRef]
33. Yano, S.; Taniguchi, T. Economically Efficient Power Storage Operation by Dealing with the Non-Normality of Power Prediction. *Energies* **2015**, *8*, 12211–12227. [CrossRef]
34. Hesse, H.C.; Martins, R.; Musilek, P.; Naumann, M.; Truong, C.N.; Jossen, A. Economic Optimization of Component Sizing for Residential Battery Storage Systems. *Energies* **2017**, *10*, 835. [CrossRef]
35. Naumann, M.; Karl, R.C.; Truong, C.N.; Jossen, A.; Hesse, H.C. Lithium-ion Battery Cost Analysis in PV-household Application. *Energy Proced.* **2015**, *73*, 37–47. [CrossRef]
36. Zakeri, B.; Syri, S. Electrical energy storage systems: A comparative life cycle cost analysis. *Renew. Sustain. Energy Rev.* **2015**, *42*, 569–596. [CrossRef]

37. Hammond, G.P.; Hazeldine, T. Indicative energy technology assessment of advanced rechargeable batteries. *Appl. Energy* **2015**, *138*, 559–571. [CrossRef]
38. Chatzivasileiadi, A.; Ampatzi, E.; Knight, I. Characteristics of electrical energy storage technologies and their applications in buildings. *Renew. Sustain. Energy Rev.* **2013**, *25*, 814–830. [CrossRef]
39. Sudworth, J.L. The sodium/nickel chloride (ZEBRA) battery. *J. Power Sources* **2001**, *100*, 149–163. [CrossRef]
40. Dustmann, C.H. Advances in ZEBRA batteries. *J. Power Sour.* **2004**, *127*, 85–92. [CrossRef]
41. Bottazzi, A.; Lamandini, C.; Manzoni, R. Pure electric and hybrid busses fleet in Bologna: 10 years experience. In Proceedings of the International Advnaced Mobility Forum (IAMF), Geneva, Switzerland, 8–9 March 2011.
42. Veneri, O.; Capasso, C.; Patalano, S. Experimental study on the performance of a ZEBRA battery based propulsion system for urban commercial vehicles. *Appl. Energy* **2017**, *185*, 2005–2018. [CrossRef]
43. Capasso, C.; Veneri, O. Laboratory bench to test ZEBRA battery plus super-capacitor based propulsion systems for urban electric transportation. *Energy Proced.* **2015**, *75*, 1956–1961. [CrossRef]
44. Yong, J.Y.; Ramachandaramurthy, V.K.; Tan, K.M.; Mithulananthan, N. A review on the state-of-the-art technologies of electric vehicle, its impacts and prospects. *Renew. Sustain. Energy Rev.* **2015**, *49*, 365–385.
45. Gaillac, L.; Skaggs, D.; Pinsky, N. Sodium nickel chloride battery performance in a stationary application. In Proceedings of the IEEE Telecommunications Energy Conference (INTELEC), Providence, RI, USA, 10–14 September 2006.
46. Zheng, M.; Meinrenken, C.J.; Lackner, K.S. Agent-based model for electricity consumption and storage to evaluate economic viability of tariff arbitrage for residential sector demand response. *Appl. Energy* **2014**, *126*, 297–306. [CrossRef]
47. Zheng, M.; Meinrenken, C.J.; Lackner, K.S. Smart households: Dispatch strategies and economic analysis of distributed energy storage for residential peak shaving. *Appl. Energy* **2015**, *147*, 246–257. [CrossRef]
48. Zhang, Y.; Lundblad, A.; Campana, P.E.; Yan, J. Employing battery storage to increase photovoltaic self-sufficiency in a residential building of Sweden. *Energy Proced.* **2016**, *88*, 455–461. [CrossRef]
49. Benato, R.; Dambone Sessa, S.; Crugnola, G.; Todeschini, M.; Turconi, A.; Zanon, N.; Zin, S. Sodium-nickel chloride (Na-NiCl 2) battery safety tests for stationary electrochemical energy storage. In Proceedings of the AEIT International Annual Conference, Capri, Italy, 5–7 October 2016.
50. Li, G.; Lu, X.; Kim, J.Y.; Lemmon, J.P.; Sprenkle, V.L. Improved cycling behavior of ZEBRA battery operated at intermediate temperature of 175 °C. *J. Power Sour.* **2014**, *249*, 414–417. [CrossRef]
51. Ao, X.; Wen, Z.; Hu, Y.; Wu, T.; Wu, X.; He, Q. Enhanced cycle performance of a Na/NiCl2 battery based on Ni particles encapsulated with $Ni_3S_2$ layer. *J. Power Sources* **2017**, *340*, 411–418. [CrossRef]
52. Antonucci, V.; Branchini, L.; Brunaccini, G.; De Pascale, A.; Ferraro, M.; Melino, F.; Orlandini, V.; Sergi, F. Thermal integration of a SOFC power generator and a Na–NiCl2 battery for CHP domestic application. *Appl. Energy* **2017**, *185*, 1256–1267. [CrossRef]
53. Li, J.; Wang, X.; Zhang, Z.; Le Blond, S.; Yang, Q.; Zhang, M.; Yuan, W. Analysis of a new design of the hybrid energy storage system used in the residential m-CHP systems. *Appl. Energy* **2017**, *187*, 169–179. [CrossRef]
54. Bindner, H.; Cronin, T.; Lundsager, P.; Manwell, J.F.; Abdulwahid, U.; Baring-Gould, I. Lifetime Modelling of Lead Acid Batteries. Risø Nat. Lab.: Roskilde, Denmark, 2005. Available online: http://orbit.dtu.dk/fedora/objects/orbit:88309/datastreams/file_7710966/content (accessed on 8 September 2017).